LEAD ISOTOPIC VARIATIONS OF THE PACIFIC AND IMPLICATIONS FOR PALEOGENE WATER MASS COMPOSITION

A Thesis

by

CRISTINA SUBT

Submitted to the Office of Graduate and Professional Studies of
Texas A&M University
in partial fulfillment of the requirements for the degree of

MASTER OF SCIENCE

Chair of Committee,	Deborah J. Thomas
Committee Members,	Franco Marcantonio
	Robert L. Korty
Head of Department,	Deborah J. Thomas

December 2013

Major Subject: Oceanography

ABSTRACT

To understand the effects changes in the meridional overturning circulation (MOC) played on past climate we need to determine where convection occurred. The late Cretaceous and early Paleogene interval (~75 to 35 Ma) was characterized by low meridional temperature gradients. Nd isotopes indicate high-latitude convection in the Pacific Ocean during this interval, with deep waters mixing in the tropical Pacific. Here we investigate the evolution of the Pb isotopic composition of water masses in the Pacific to constrain variability in weathering inputs into the inferred convection regions from ~75 to 35 Ma. We generated $^{206,207,208}Pb/^{204}Pb$ isotope records for North Pacific DSDP and ODP Sites 192, 464, and 883, and South Pacific DSDP Sites 323, 463, and 596.

$^{206}Pb/^{204}Pb$ trends differ from $^{207,208}Pb/^{204}Pb$ values, which typically show similar trends to each other—resulting from the mixing of multiple Pb sources. North Pacific sites typically exhibit relatively lower Pb compositions than South Pacific, and evidence from detrital analyses suggests sources of Pb to North Pacific sites received strong contributions of continental dust. Pb and Nd are coupled in North Pacific sites between ~62 and 50 Ma, as well as in the Southern Ocean throughout the study period, indicating the Pb composition in this region was influenced by the composition of advected deep water masses. North Pacific sites also show decoupling of Pb and Nd ~50 Ma, during the Early Eocene Climatic Optimum (EECO), which may be indicative of more distal

South Pacific deep waters increasing in contributions. Pb composition in the subtropical South Pacific also suggests a stronger influence of dust dissolution whereas the Nd composition was dominated by water mass composition. North Pacific Pb values may also have reflected shifting sources during the EECO. The Pb and Nd composition at Site 883 shows a short radiogenic excursion in Pb values ~40 Ma, possibly cased by a short period of strengthened North Pacific Deep Water (NPDW) influence on the isotopic composition during the Mid-Eocene Climatic Optimum (MECO).

Para Bapu, Lita y Normilu

ACKNOWLEDGEMENTS

I would like to offer my sincerest thanks to my advisor and committee chair, Dr. Debbie Thomas, who has never failed to provide expert guidance and valuable advice. I would also thank my committee members, Drs. Franco Marcantonio and Robert Korty, as well as Dr. Brent Miller, for his assistance with the TIMS and Pb chemistry, and to Luz Romero, for lab support.

Funding for this research was provided through the National Science Foundation. Personal funding was provided through an ODASES Fellowship and through a Science Technology Engineering and Math scholarship. Special thanks go to Ken Williams for his support of the R. Ken Williams ’45 Radiogenic Isotope Geosciences Laboratory. Samples and their data were provided by the Integrated Ocean Drilling Program, funded in part by the National Science Foundation.

I am also indebted to all my family and friends, who have provided endless support and guidance over the years. Their encouragement and patience saw me through the bad days, late nights, and tough times, and I will never forget it.

NOMENCLATURE

Elements

Fe	Iron
Mn	Manganese
Nd	Neodymium
Pb	Lead
Sr	Strontium
Th	Thorium
U	Uranium

Units

$\varepsilon_{Nd}(t)$	Age corrected epsilon notation of Nd isotopic ratios
Ma	Milliannum
MBSF	Meters below sea floor
Myr	Million years

Miscellaneous

CCD	Carbonate compensation depth
DSDP	Deep Sea Drilling Program
EECO	Early Eocene Climatic Optimum
MECO	Middle Eocene Climatic Optimum
MOC	Meridional Overturning Circulation

MORB	Mid-ocean ridge basalts
NADW	North Atlantic Deep Water
NPDW	North Pacific Deep Water
NIST	National Institute of Standards and Technology
ODP	Ocean Drilling Program
SPDW	South Pacific Deep Water
SST	Sea surface temperature
TIMS	Thermal Ionization Mass Spectrometer

TABLE OF CONTENTS

LIST OF FIGURES

LIST OF TABLES

TABLE Page

1. INTRODUCTION

The Late Cretaceous and Early Paleogene (~75-45 Ma) were characterized by overall warmth, and represent the last major greenhouse climate interval [*Bains et al.*, 1999; *Pearson and Palmer*, 2000; *Zachos et al.*, 2001]. Estimates for atmospheric CO_2 during this period vary 3 to 5 times preindustrial levels, but are commonly agreed to have been higher than modern levels [*Bice et al.*, 2006; *Pearson and Palmer*, 2000]. Higher estimated greenhouse gas concentrations during this time are consistent with higher sea surface temperatures (SSTs) reconstructed for the time period. These SSTs range from ~36°C at the equator, to ~21° and ~14°C at the Arctic and Antarctic regions, respectively, between 55 and 48 Ma [*Bijl et al.*, 2009]. The resulting reconstructed meridional temperature gradient during the Paleogene was significantly lower than modern gradients. Estimates of abyssal water temperatures (~7-12°C from 65 to 45 Ma) suggest that the vertical gradient of temperature would also have been weaker in the Paleogene [*Bijl et al.*, 2009; *Huber et al.*, 2002; *Zachos et al.*, 2008].

The meridional overturning circulation (MOC) is a principal component of oceanic heat transport in the modern climate system. It consists of an upper northward flow of warm water, compensated by deep-water flow southward in the Atlantic Ocean known as the North Atlantic Deep Water (NADW). A stronger than average overturning relates to larger northward heat transport; therefore, it results in higher surface air temperatures and humidity in the Northern Hemisphere. Variability in the MOC on decadal timescales influences temperate climates found in the North Atlantic and European sectors during summer months [*Msadek and Frankignoul*, 2009; *Pohlmann et*

al., 2006]. There is however, uncertainty in the strength of this influence and its role in the heat transport to higher latitudes [*Bryden et al.*, 2005; *McPhaden and Zhang*, 2002]. On geologic timescales, the strength of pole-to-equator temperature gradients is classically assumed to affect the strength of the MOC [*Bice et al.*, 2006; *Bijl et al.*, 2009; *Christensen et al.*, 1997]. Therefore, if we assume the MOC's influence on climate depends on its strength, we can infer it would have been even weaker during the Cretaceous and Paleogene, when horizontal and vertical temperature gradients were lower than at present [*Bijl et al.*, 2009].

In order to understand the role of the MOC in ancient climate, we need to reconstruct the plate distribution and placements during our study period. Tectonic differences in ocean basin configuration likely impacted the pattern of MOC during the Late Cretaceous and Early Paleogene. In the North Atlantic, the continental breakup that led to the formation of the Labrador Sea occurred ~80 Ma [*Le Pichon et al.*, 1971]. Moreover, formation of the Norwegian-Greenland Sea also began during the Early Paleogene and lasted until ~50 Ma [*Olesen et al.*, 2007; *Talwani and Eldholm*, 1977; *Torsvik and Cocks*, 2005]. The Atlantic Ocean was a considerably smaller basin than it is today, and both northern North Atlantic basins were only beginning to open during the Late Cretaceous and Early Paleogene, thus convection of deep waters in the North Atlantic was unlikely [*Pak and Miller*, 1992; *Thomas et al.*, 2003; *Via and Thomas*, 2006]. The Drake Passage was closed during the early Paleogene, restricting the flow of deep waters around South America [*Barker and Burrell*, 1977; *Livermore et al.*, 2005]; its opening did not occur until the Eocene/Oligocene boundary [*Barker*, 2001; *Lawver*

and Gahagan, 2003]. The opening of the Tasman Gateway between Australia and Antarctica, which did not occur until ~35 to 30 Ma, would have impacted the transport around Australia [*Stickley et al.*, 2004], and together with the opening of the Drake Passage, also formed the circum-Antarctic seaway. By ~32 Ma, the circum-Antarctic had an unrestricted opening deeper than 2000 m. [*Lawver and Gahagan*, 2003] and is often linked to the transition from the Early Cenozoic warm period to the Late Cenozoic cooling period [*Murphy and Kennett*, 1986; *Shackleton and Kennett*, 1974; *Zachos et al.*, 1996]. At lower latitudes, the Panama Isthmus did not close until fairly recently (~4.2 Ma) and until then, some exchange of surface and intermediate waters may have occurred [*Coates et al.*, 1992; *Haug et al.*, 2001]. The closing of the Tethys Sea and the subsequent opening of the Indian Ocean, began in the Late Cretaceous and completed ~50 to 40 Ma [*Coleman*, 1981; *Searle et al.*, 1987; *Ziegler*, 1987].

Reconstructions of the pattern of MOC during the late Cretaceous and Early Paleogene using Nd isotopes indicate a bipolar convection system in the Pacific, where sinking occurred at high latitudes in both hemispheres (Fig. 1.1) [*Christensen et al.*, 1997; *Hague et al.*, 2012; *Thomas et al.*, 2008; *Thomas et al.*, in review]. These two deep-water masses likely mixed in the tropical regions of the Pacific. Moreover, the data also suggest the possibility of Pacific MOC being independent of the Atlantic until ~37 Ma [*Thomas et al.*, 2008]. At this time, the opening of the Drake Passage would have allowed for mixing of the relatively radiogenic $\varepsilon_{Nd}(t)$ values from the Pacific with the relatively unradiogenic values of the Atlantic, causing a convergence in values shortly thereafter (~40 Ma) [*Scher and Martin*, 2004; *Thomas et al.*, in review].

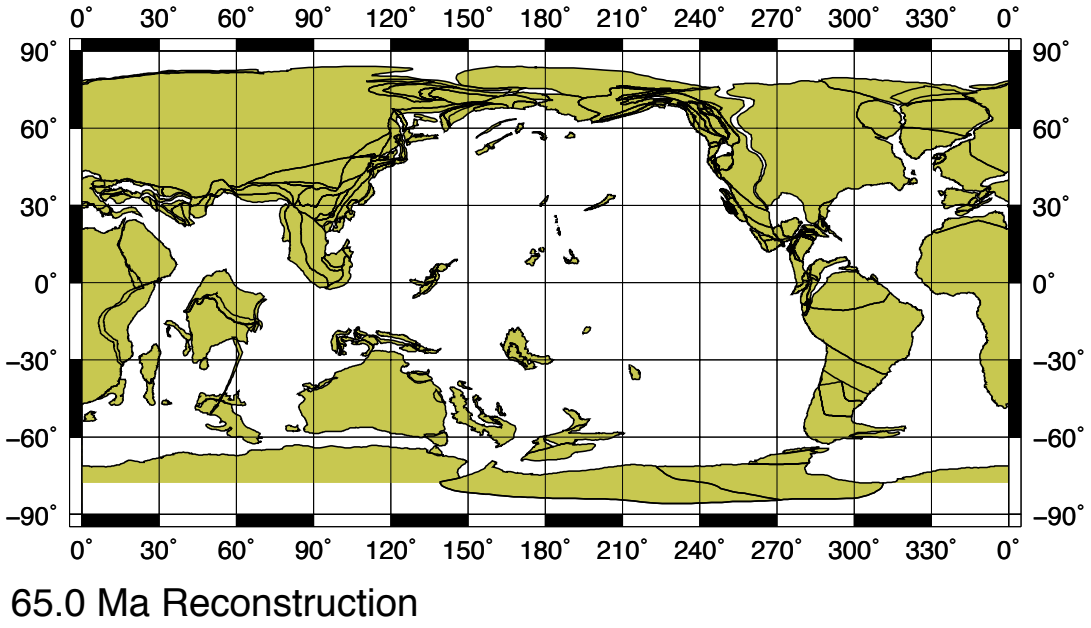

Figure 1.1 Plate tectonic reconstruction for 65 Ma. This map was generated using the Ocean Drilling Stratigraphic Network (http://www.odsn.de).

While a growing body of Nd isotope data is beginning to constrain the mode and pattern of MOC during the Late Cretaceous and Early Paleogene, important details of the MOC evolution and its response to regional or global climate change need to be determined. The aim of this study is to reconstruct the Pb isotopic composition of seawater in the North and South Pacific during ~70 to 30 Ma. Pb has a shorter residence time in the oceans than Nd, therefore it is useful for tracking changes in the weathering inputs into regions of convection [*Foster and Vance*, 2006; *Frank*, 2011; *van de Flierdt et al.*, 2003].

2. BACKGROUND

2.1 Pb Isotopes

Reconstructions of the Pb isotopic composition of ancient water masses involve the 4 isotopes of Pb. ^{206}Pb, ^{207}Pb and ^{208}Pb are all radiogenic nuclides and are the final daughter products of ^{238}U, ^{235}U, and ^{232}Th with half-lives of 4.468 x10^{9}, 7.038 x10^{8}, and 1.401 x10^{10} years, respectively. Each of these is normalized to ^{204}Pb, which is stable and not radiogenic. Radiogenic Pb is found in igneous rocks with high U/Pb and Th/Pb ratios that are old enough for significant amounts of Pb to be produced from U and Th decay. Typically, older continental source rocks are characterized by radiogenic Pb values while younger volcanic sources depict more unradiogenic Pb [*Pettke et al.*, 2002].

2.2 Pre-anthropogenic Pb in Seawater

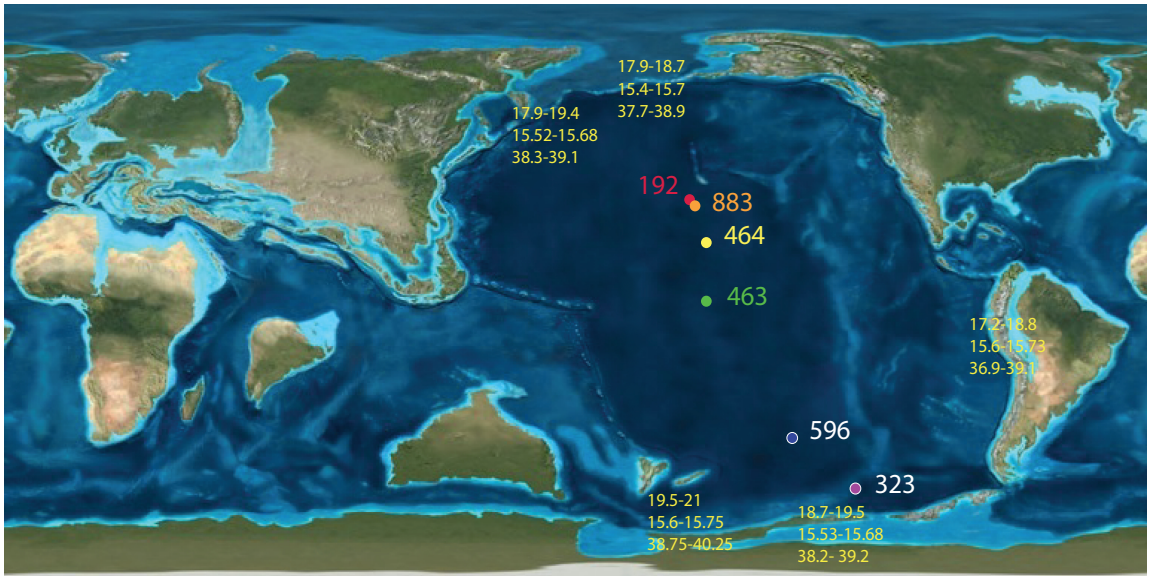

Figure 2.1 Typical Pb values of source rocks surrounding the Pacific basin. Pb range values shown in yellow: $^{206}Pb/^{204}Pb$ top, $^{206}Pb/^{204}Pb$ middle, and $^{206}Pb/^{204}Pb$ bottom. Reconstruction map represents tectonic arrangements ~65 Ma (Ron Blakey, Colorado Plateau Geosystems, Ariz. USA).

Pb isotope compositions of different water masses vary geographically and chronologically. This is due to variations in the geographic distribution of exposed source rocks. Existing seawater Pb isotope records indicate less radiogenic Pb in the Pacific than the Atlantic, mostly due to the widely differing sources [*von Blanckenburg et al.*, 1996]. Volcanic rocks from mid ocean ridges (MORB) typically have Pb isotope compositions with low radiogenic values ($^{206}Pb/^{204}Pb$ ratios between 18.1 and 18.4, $^{207}Pb/^{204}Pb$ ratios between 15.4 and 15.5, and $^{208}Pb/^{204}Pb$ ratios between 37.6 and 38.0) [*Sun*, 1980]. Figure 2.1 shows typical Pb isotope compositions of likely source rocks surrounding the Pacific Ocean. Exposed rocks in the North Pacific are predominantly volcanic, such as the Alaskan and Aleutian arcs, which have been active since ~75 Ma [*Moll-Stalcup*, 1994], and a section of the Kuril arc active through the study interval [*Konstantinovskaia*, 2001]. North Pacific ocean islands arcs, whose exposed rocks mainly contain basalts, and andesites, generally have a larger overall range ($^{206}Pb/^{204}Pb$ ratios between 17.9 and 18.7, $^{207}Pb/^{204}Pb$ ratios between 15.4 and 15.7, and $^{208}Pb/^{204}Pb$ ratios between 37.7 and 38.9) [*Sun*, 1980]. However, the Pacific continental arcs have much higher variability in $^{206}Pb/^{204}Pb$ ratios (between 17.9 and 19.4), but lower for $^{207}Pb/^{204}Pb$ and $^{208}Pb/^{204}Pb$ ratios (15.52 to 15.68, and 38.3 to 39.1, respectively) [*von Blanckenburg et al.*, 1996]. Antarctic exposed rocks also have high Pb isotope compositions with strong variability that can depend on location. For example, in the Antarctic Peninsula alkali basalts, $^{206}Pb/^{204}Pb$ ratios are generally between 18.8 and 19.5, $^{207}Pb/^{204}Pb$ ratios are between 15.55 and 15.65, and $^{208}Pb/^{204}Pb$ ratios fall between 38.5 and 39 [*Finn et al.*, 2005; *Hole et al.*, 1993]. Pb values from Marie Byrd Land and other

West Antarctic tills however, are much higher ($^{206}Pb/^{204}Pb$ ratios between 19.5 and 21, $^{207}Pb/^{204}Pb$ ratios between 15.6 and 15.75, and $^{208}Pb/^{204}Pb$ ratios between 38.75 and 40.25)[*Finn et al.*, 2005; *Lang Farmer et al.*, 2006]. Lithology of West Antarctic exposures is not very well known, but includes Late Paleozoic and Mesozoic basement rocks like the Ford Granodiorite and the Byrd Coast Granite [*Wilson*, 1992]. In contrast, the East Antarctic tills, consisting mostly of various volcanic facies, have lower Pb values ($^{206}Pb/^{204}Pb$ ratios between 18.36 and 18.64, $^{207}Pb/^{204}Pb$ ratios between 15.59 and 15.63, and $^{208}Pb/^{204}Pb$ ratios between 38.643 and 39.18) [*Lang Farmer et al.*, 2006].

Dissolved Pb is supplied to the oceans predominantly through riverine inputs and atmospheric dust dissolution [*Duce et al.*, 1991; *Frank*, 2002; *Henderson and Maier-Reimer*, 2002; *Jones et al.*, 2000]. The intensity of weathering may impact the Pb isotopic composition of the rivers, and hence the ocean. The weathering of continental rocks such as zircon, apatite, and sphene can cause fractionation of Pb isotopes when these minerals are damaged by radioactive decay. Thus, the daughter isotopes become more loosely bound in the crystal structure and are more easily mobilized during weathering as opposed to nonradiogenic ^{204}Pb [*Erel et al.*, 1994; *Jones et al.*, 2000]. Eolian inputs are significant in areas where fluvial inputs are minimal, usually in regions far from land [*Jones et al.*, 2000; *Ling et al.*, 2005]. This is an aspect of Pb marine geochemistry that is different from Nd, which does not reflect significant eolian inputs [*Jones et al.*, 1994]. The increasingly humid climate of the Late Cretaceous and Paleocene would have limited the amount of material available for erosion and thus, eolian deposition [*Janecek and Rea*, 1983]. Volcanic ash may also contribute as a

source of dissolved Pb to seawater, similar to continental dust [*Patterson and Settle*, 1987]. Although the particulate material emitted from hydrothermal vents contains high amounts of Pb and other metals [*Trocine and Trefry*, 1988], the contribution of Pb in seawater from hydrothermal vents is negligible due to the particle reactive nature of Pb in seawater [*Barrett et al.*, 1987]. However, modern Pb marine geochemical cycling is difficult to quantify due to significant anthropogenic alteration of the natural sources and sinks [*Nriagu*, 1989; *Shen and Boyle*, 1988].

The oceanic residence time of Pb has been estimated using the particle reactivity and concentrations of the short-lived, radioactive ^{210}Pb [*Cochran et al.*, 1990; *Craig et al.*, 1973; *Henderson and Maier-Reimer*, 2002]. Estimates of the residence time vary from 50 to 100 years, and are short relative to the nominal rate of oceanic mixing (~1500 years) [*Broecker et al.*, 1960]. Pb is readily adsorbed onto particulates in seawater upon being introduced or produced from their parent nuclides, thus it is also rapidly removed [*Henderson and Maier-Reimer*, 2002; *Tanaka et al.*, 1983]. The short residence time of Pb allows it to be especially sensitive to rapid or transient weathering inputs, especially in relation to wind provenance [*Abouchami et al.*, 1997]. The variations in the composition of Pb isotopes are mainly dependent upon the riverine inputs, where Pb is derived from rock weathering [*Goldstein and Jacobsen*, 1988]. Small, localized variations in Pb reflect the different inputs from sources or the general ocean circulation pattern [*Abouchami et al.*, 1997].

3. SAMPLES AND METHODS

3.1 Site Selection and Age Control

The selected sites, as shown in Figure 3.1, have been investigated previously for seawater Nd isotopic reconstructions.

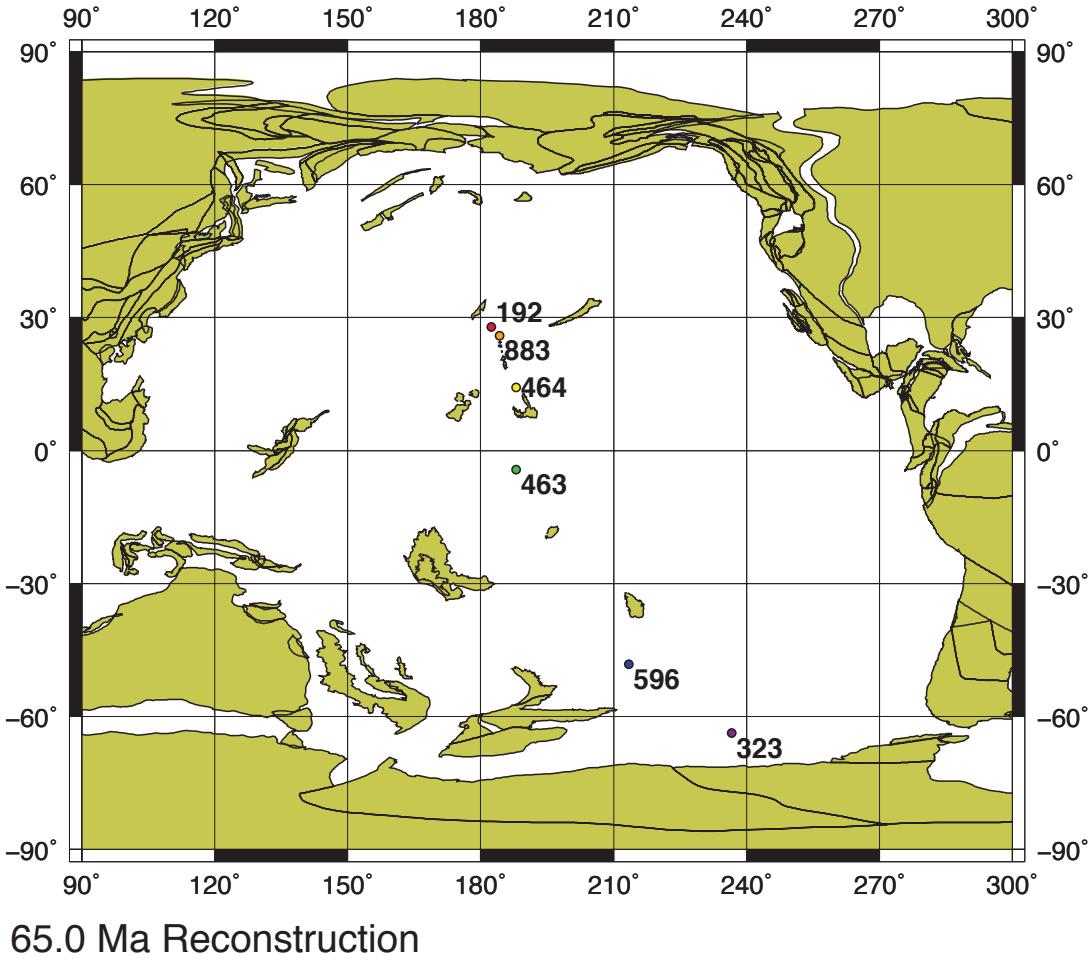

Figure 3.1 Plate tectonic reconstruction of Pacific 65 Ma showing study sites. This map was generated using the Ocean Drilling Stratigraphic Network (http://www.odsn.de/).

3.1.1 DSDP Site 192, Hole 192A (Meiji Guyot)

Hole 192A (Leg 19) is the northernmost site in the study, with a paleolatitude of 40°N, and a paleodepth of 2500 m. Ages for these samples were determined using available carbonate microfossils found in the sediments [*Creager et al.*, 1971], and were assigned to ages as defined by Gradstein et al. [2004]. The study interval spans ages from the Maastrichian to the late Eocene. Previous research indicates an unconformity ranging from Paleocene to Early Eocene [*Creager et al.*, 1971]. Analysis of this site may provide Pb values for weathered material of rocks from exposed arc volcanics in the North Pacific.

3.1.2 ODP Site 883, Hole 883B (Detroit Seamount)

Hole 883B is part of Site 883 (Leg 145) and is positioned on the Detroit Seamount with a paleodepth of 2000 m and a paleolatitude of 32°N. It spans from the Maastrichian to the late Eocene. Ages at this site were determined using available carbonate microfossils found in the sediments [*Rea et al.*, 1993]. Numerical ages were assigned from Gradstein et al. [2004]. Site 883 records the highest $\varepsilon_{Nd}(t)$ values in this study interval with peak values of +3.7 at 61.6 Ma, and leveled off ca. 52 Ma. This, along with the radiogenic $\varepsilon_{Nd}(t)$ values found at Site 464, suggests a source of radiogenic sediments from the North and Northwest of the study sites. The Pb isotope record can provide further information about the source regions for this site.

3.1.3 DSDP Site 464, Hole 464 (Northern Hess Rise)

Hole 464 (Leg 62) is located on the Northern Hess Rise. It has a paleodepth of 4000 m and a paleolatitude of 18°N [*Thiede et al.*, 1981]. Its ages span from the late

Cretaceous to the late Eocene. Sediments in this region consist mostly of red clays with essentially no biostratigraphic control. Age control was assigned by using the closest biostratigraphic datums above and below the study interval, resulting in datums ranging from 75 to 2.8 Ma (89.0 and 32.0 mbsf respectively). Linear interpolation between these datums produced ages too young throughout the section, which conflicted with the ichthyolith stratigraphy [*Doyle and Riedel*, 1981]. Thus the most precisely identified ichthyolith was included (50.0 mbsf) and was assigned a datum (55.8 Ma) based on the Paleocene-Eocene boundary age from Gradstein et al. [2004]. The Nd record for this site is highly variable, though significantly more radiogenic than the Southern sites. It also indicates more radiogenic Nd values than other Northern sites cored at shallower depths, helping to constrain the influence of the bathymetric control [*Hague et al.*, 2012].

3.1.4 DSDP Site 463, Hole 463 (Mid Pacific Mountains)

Hole 463 (Leg 62), found in the Mid-Pacific Mountains has a paleolatitude at the equator, and a paleodepth of 2000 m. The core spans ages from the Maastrichian to the late Eocene. This site was cored in a region above the CCD, which preserved the calcareous sediments. However, the core includes two unconformities within the study interval [*Thiede et al.*, 1981], making biostratigraphic control particularly difficult, therefore Sr isotopes [*Barrera et al.*, 1997] were converted to ages using McArthur's [2001] Look-Up Table Version 4:08/04 [*Thomas et al.*, in review]. There are two large hiatuses that limit the availability of stratigraphic data during the study time interval. One ~17 Myr hiatus exists spanning the entire Paleocene, and a second hiatus occurs

encompassing most of the Eocene and the lower Oligocene. The Nd record of this site suggests this was a region of water mass mixing between the North and South Pacific deep waters. Since this site is not in a region near land, Pb sources are expected to be mostly from dust input.

3.1.5 DSDP Site 596, Hole 596 (Southwest Pacific)

Hole 596 (Leg 91) can be found in the Southwest Pacific, with a paleodepth of 5000 m and a paleolatitude of 38°S. It spans the late Cretaceous to the late Eocene (~54-62 Ma). The sediments consist mostly of brown clays which lack biostratigraphically useful microfossils [*Menard et al.*, 1987]. Co and Ir accumulation models were constructed by Zhou and Kyte to determine the clay sequence and produced a refined age model for site 596 [1992]. This age model uses the Ir peak at the K/T boundary, therefore ages were updated to the GTS 2004 by adjusting the K/T age (constant offset of -0.9 Myr) [*Thomas et al.*, in review]. The Nd record of this site was fairly constant throughout the study interval with an average deep water $\varepsilon_{Nd}(t)$ value of -5.5. The constancy of these values suggests the water mass had little to no change over the long-term study interval. The Pb isotope record can give evidence of short-term weathering events that may have occurred, not recorded by the Nd record.

3.1.6 DSDP Site 323, Hole 323 (Bellinghausen Abyssal Plain)

Hole 323 (Leg 35) is the southernmost site in the study, and is found in the Bellinghausen abyssal plain, at a paleolatitude of 65°S, and a paleodepth of 4000 m [*Hollister et al.*, 1976]. The study interval spans ages from the Maastrichian to the Eocene. The lithology of the study section is mostly composed of red clays, devoid of

microfossils [*Rögl et al.*, 1976], making it difficult to determine an age model. Therefore, the closest biostratigraphic datums above and below the clay interval being studied were applied and constant accumulation rates were assumed using typical Pacific accumulation rates of red clays. A hiatus interval occurs in the sediments at Site 323 spanning most of the Eocene, therefore the age model for this site can only be considered as a broad estimate [*Hollister et al.*, 1976].

3.2 Analytical Methods

The bulk sample, taken at 1-2 cm. increments from selected cores, is dried and homogenized before beginning chemistry. Sample preparation followed the methods of Martin et al. [2010] and Basak et al. [2011], in which a Na acetate buffer made of 1M Na acetate (52%) and 1 M acetic acid (48%) and 10 mL of cation exchange resin to remove any Pb contamination from the buffer should be used to soak the sediment for 2 hrs. and decarbonate each sample (the resin should not be mixed with the sample). After centrifuging and rinsing 3 times with ultrapure deionized water (18.2 Milli-Q), the oxide fraction is extracted by leaching the samples in a .02 M Hydroxylamine Hydrochloride (HH) solution in 20% acetic acid buffered to pH 4. Pb isolation follows the methods of Lugmair & Galer [1992], in which the aliquot is fluxed through columns with standard HBr chemistry. For selected samples, the remainder of the sediment is leached again to extract the detrital fraction, then dissolved in a HF-HNO_3 mixture.

Pb analysis acquires all three ratios ($^{206}Pb/^{204}Pb$, $^{207}Pb/^{204}Pb$, $^{208}Pb/^{204}Pb$), using the Thermo Triton Thermal Ionization Mass Spectrometer (TIMS) of the R. Ken Williams ’45 Radiogenic Isotope Geosciences Laboratory at Texas A&M University.

The samples are loaded onto single Re filaments using silica gel and phosphoric acid. The ionization temperature is consistently kept within 1251±4°C. 20 NIST 981 63µg/mg Pb standards are used to determine fractionation values. The average fractionation value for standards is .085% per amu with a standard deviation of .01% per amu. Pb isotopic ratios were corrected for mass fractionation by normalizing to $^{206}Pb/^{204}Pb=16.9356$, $^{207}Pb/^{204}Pb=15.4891$, and $^{208}Pb/^{204}Pb=36.7006$ [*Todt et al.*, 1996]. Blanks were spiked with 5 µl of a ^{208}Pb tracer and yielded total Pb blanks within the range of 6.72±2.69 pg, and 1.345±.535 pg blank per 5 µl.

4. RESULTS

The following results and corresponding graphs in Figures 4.1 to 4.6 are presented in geographic order from North to South. We analyzed a total of 82 leached oxide samples from Sites 192 (8 samples), 883 (17 samples), 464 (21 samples), 463 (4 samples), 596 (17 samples), and 323 (15 samples), and an additional 12 detrital analyses from samples at Sites 192 (2 samples), 883 (3 samples), 464 (3 samples), 596 (2 samples), and 323 (2 samples).

4.1 Site 192- Paleolatitude 40°N, Paleodepth 2500 m

Site 192 (Fig. 4.1) seawater $^{206}Pb/^{204}Pb$ values decrease from 18.3 to 18.1 over the interval 1023.02 to 1020.42 mbsf, then increase gradually from 18.1 to 18.2 over the interval 1020.42 to 959.07 mbsf, then increase to 18.8 at 945.51 mbsf. The corresponding $^{207}Pb/^{204}Pb$ values remain constant at 15.6 over the interval 1023.02 to 985.02 mbsf, increase to 15.7 at 959.07 through 951.66 mbsf, then decrease gradually to 15.6 at 945.51 mbsf. And the $^{208}Pb/^{204}Pb$ values decrease from 38.3 to 38.0 over the interval 1023.02 to 1020.42 , then increase at an exponential pace from 38.0 to 38.7 between 1020.42 to 951.66 mbsf, then decrease gradually to 38.5 at 945.51 mbsf.

We analyzed the detrital Pb isotopic composition of two samples at Site 192. The values at 1020.42 mbsf were 18.5, 15.5, and 38.3 for the $^{206}Pb/^{204}Pb$, $^{207}Pb/^{204}Pb$, and $^{208}Pb/^{204}Pb$ values respectively. The values at 945.51 mbsf were 18.9, 15.7, and 38.9 for the $^{206}Pb/^{204}Pb$, $^{207}Pb/^{204}Pb$, and $^{208}Pb/^{204}Pb$ values respectively.

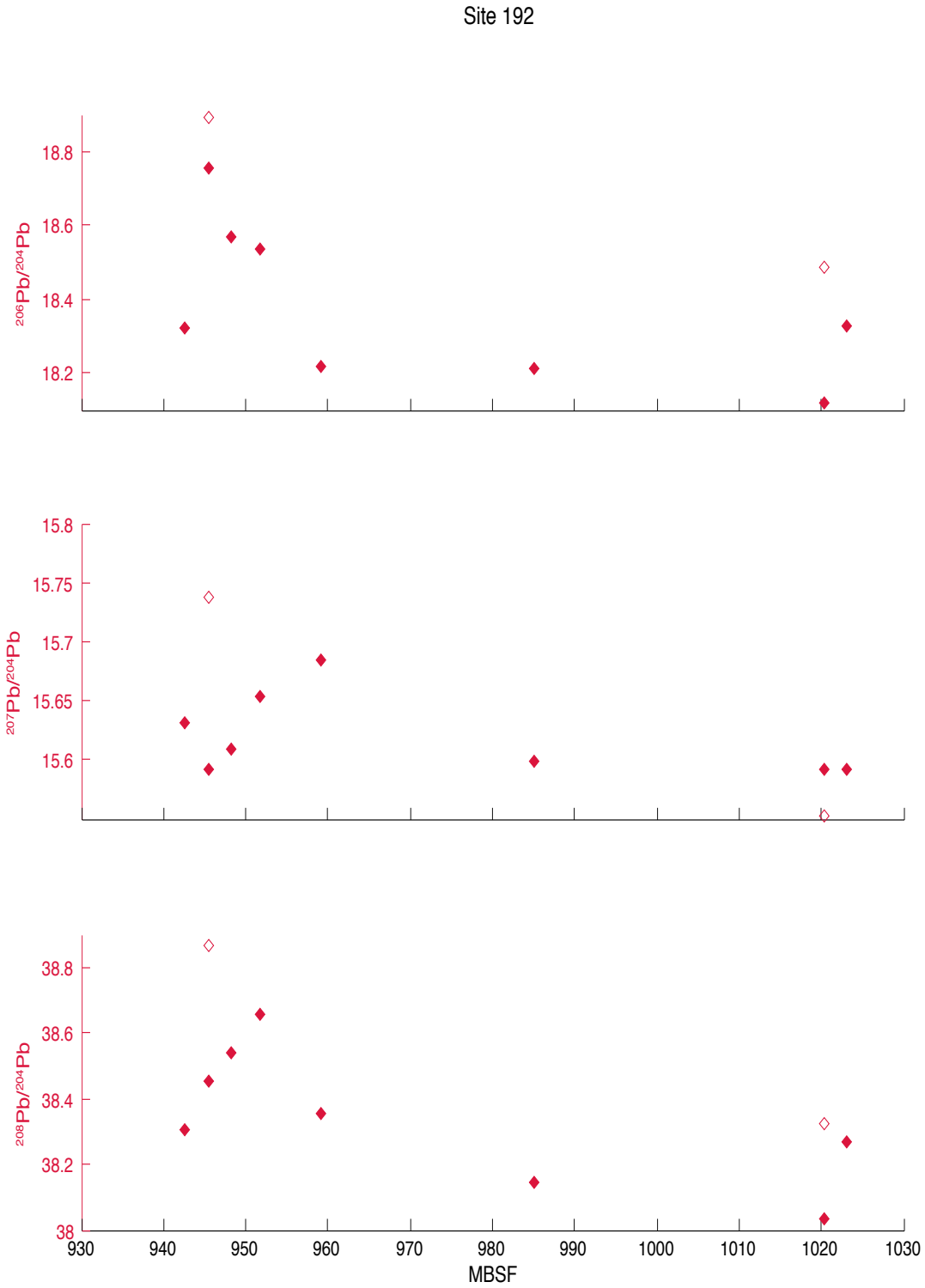

Figure 4.1 Pb isotopic data generated from Site 192. Open symbols represent detrital Pb values.

4.2 Site 883- Paleolatitude 32°N, Paleodepth 2000 m

Site 883 (Fig. 4.2) seawater $^{206}Pb/^{204}Pb$ values decrease from 18.6 to 18.4 over the interval 829.07 to 824.55 mbsf, increase gradually to 18.8 at 789.68 mbsf, decrease to 18.3 at 787.20 through 751.20 mbsf, then increase to 18.8 at 734.9 mbsf and decrease to 18.2 at 730.18 through 727.02 mbsf. The corresponding $^{207}Pb/^{204}Pb$ values decrease from 15.72 to 15.58 over the interval 829.07 to 824.55 mbsf, remain constant at 15.62 from 820.2 to 813.6 mbsf, increase to 15.64 at 809.5 through 789.68 mbsf, then decrease to 15.6 at 787.20 through 779.80, then increase to 15.64 at 753.15, decrease to 15.58 at 751.20 mbsf, then increase to at 734.90 mbsf and decrease to 15.59 at 730.18 through 727.02 mbsf. The $^{208}Pb/^{204}Pb$ values decrease from 38.9 to 38.3 over the interval 829.07 to 824.55 mbsf, then increase gradually to 38.7 at 809.5 mbsf. Values then decrease gradually to 38.2 at 785.70 through 783.32 mbsf, increase to 38.4 at 781.2, decrease to 38.3 at 779.80 through 751.20, then decrease to 38.6 at 734.9 mbsf before decreasing to 38.1 at 730.18 through 727.02 mbsf.

We analyzed the detrital Pb isotopic composition of three samples at Site 883. The values at 824.55 mbsf were 18.5, 15.61, and 38.5 for the $^{206}Pb/^{204}Pb$, $^{207}Pb/^{204}Pb$, and $^{208}Pb/^{204}Pb$ values respectively. The values at 753.15 mbsf were 18.6, 15.63, and 38.6 for the $^{206}Pb/^{204}Pb$, $^{207}Pb/^{204}Pb$, and $^{208}Pb/^{204}Pb$ values respectively. The values at 730.21 mbsf were 18.5, 15.61, and 38.5 for the $^{206}Pb/^{204}Pb$, $^{207}Pb/^{204}Pb$, and $^{208}Pb/^{204}Pb$ values respectively.

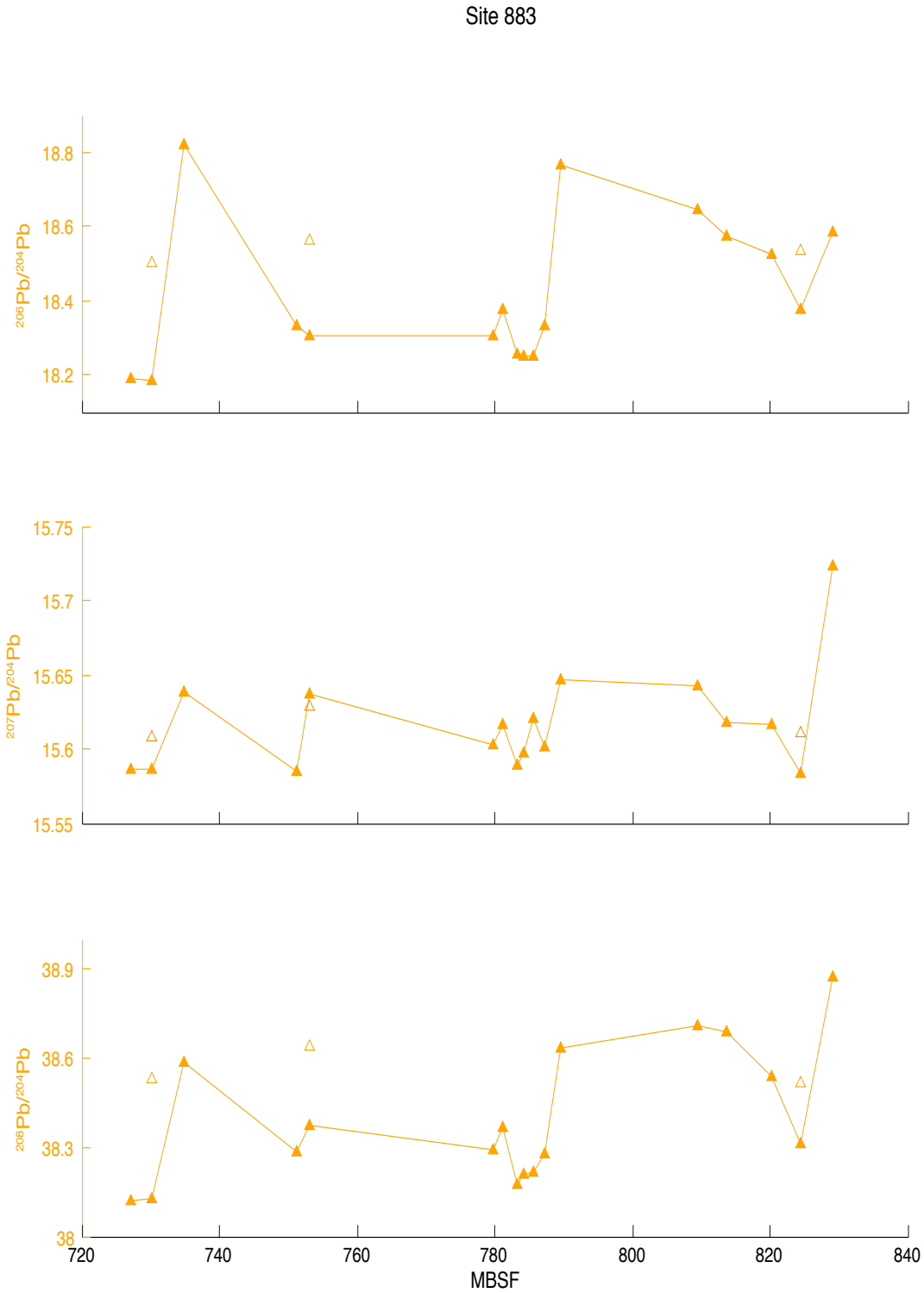

Figure 4.2 Pb isotopic data generated from Site 883. Open symbols represent detrital Pb values.

4.3 Site 464- Paleolatitude 18°N, Paleodepth 4000 m

Site 464 (Fig. 4.3) seawater $^{206}Pb/^{204}Pb$ values decrease from 18.59 to 18.55 over the interval 73.86 to 71.95 mbsf, then increase to 19.1 at 70.04 mbsf and decrease to 18.7 at 62.16 mbsf. Values remain between 18.55 and 18.62 over the interval 62.02 to 53.5 mbsf, then increase to 18.7 at 53.1 mbsf, then remain between 18.6 and 18.66 over the interval 52.25 to 48.55 mbsf, then increase to 18.9 at 47.76 mbsf, and decrease gradually to 18.6 over the interval at 42.40 mbsf. The corresponding $^{207}Pb/^{204}Pb$ values decrease from 15.64 to 15.60 over the interval 73.86 to 71.95 mbsf, then increase to 15.72 at 70.04 mbsf and decrease to 15.65 at 62.16 mbsf. Values remain at 15.6 over the interval 62.02 and 56.2, then increase to 15.63 at 55.37 mbsf and decrease again to 15.61 at 53.5 mbsf, then rise exponentially to 15.66 at 49.64, and repeated runs at 48.55 mbsf yield values of 15.73 and 15.63. Values then increase to 15.68 at 47.95 through 45.50, and decrease gradually to 15.63 at 42.4 mbsf. The $^{208}Pb/^{204}Pb$ values decrease from 38.5 to 38.3 over the interval 73.86 to 71.95 mbsf, then increase to 38.8 at 70.04 mbsf and decrease to 38.7 at 62.16 mbsf. Values remain between 38.52 and 38.57 over the interval 62.02 to 56.20 mbsf, then increase to 38.7 at 55.37 mbsf and return to 38.5 and remain between 38.5 and 38.6 over the interval 53.50 to 51.50 mbsf, and increase to 38.7 at 49.64 mbsf. At 48.55 mbsf, repeated runs yield values of 39.0 and 38.7. Values increase to 38.8 at 47.95 through 43.97 mbsf, and decrease gradually to 38.7 at 42.4 mbsf.

We analyzed the detrital Pb isotopic composition of three samples at Site 464. The values at 62.16 mbsf were 18.7, 15.61, and 38.7 for the $^{206}Pb/^{204}Pb$, $^{207}Pb/^{204}Pb$, and

$^{208}Pb/^{204}Pb$ values respectively. The values at 45.5 mbsf were 18.8, 15.7, and 39.0 for the $^{206}Pb/^{204}Pb$, $^{207}Pb/^{204}Pb$, and $^{208}Pb/^{204}Pb$ values respectively. The values at 42.40 mbsf were 18.8, 15.66, and 39.0 for the $^{206}Pb/^{204}Pb$, $^{207}Pb/^{204}Pb$, and $^{208}Pb/^{204}Pb$ values respectively.

4.4 Site 463- Paleolatitude 0°, Paleodepth 2000 m

Site 463 (Fig. 4.4) seawater $^{206}Pb/^{204}Pb$ values decrease from 18.5 to 18.2 over the interval 53.4 to 46.23 mbsf, then increase to 18.6 at 43.98 mbsf, then decrease to 18.3 at 41.41 mbsf. The corresponding $^{207}Pb/^{204}Pb$ values decrease from 15.63 to 15.62 over the interval 53.4 and 46.23 mbsf, then increase to 15.66 at 43.98 mbsf, then decrease to 15.62 at 41.41 mbsf, and the $^{208}Pb/^{204}Pb$ values decrease from 38.2 to 38.1 over the interval 53.4 to 46.23 mbsf, then increase to 38.3 at 43.98 mbsf, and decrease to 38.25 at 41.41 mbsf.

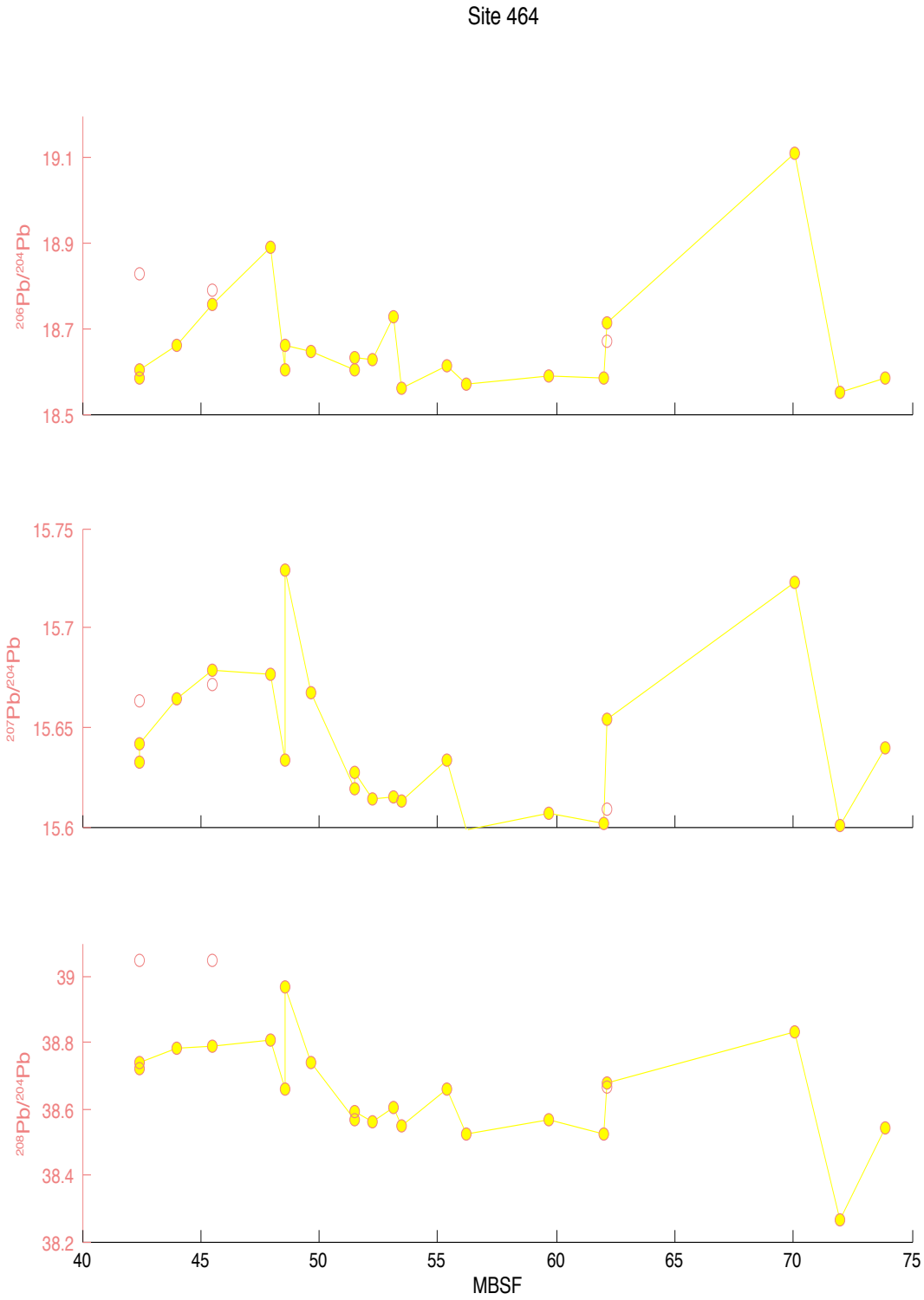

Figure 4.3 Pb isotopic data generated from Site 464. Open symbols represent detrital Pb values.

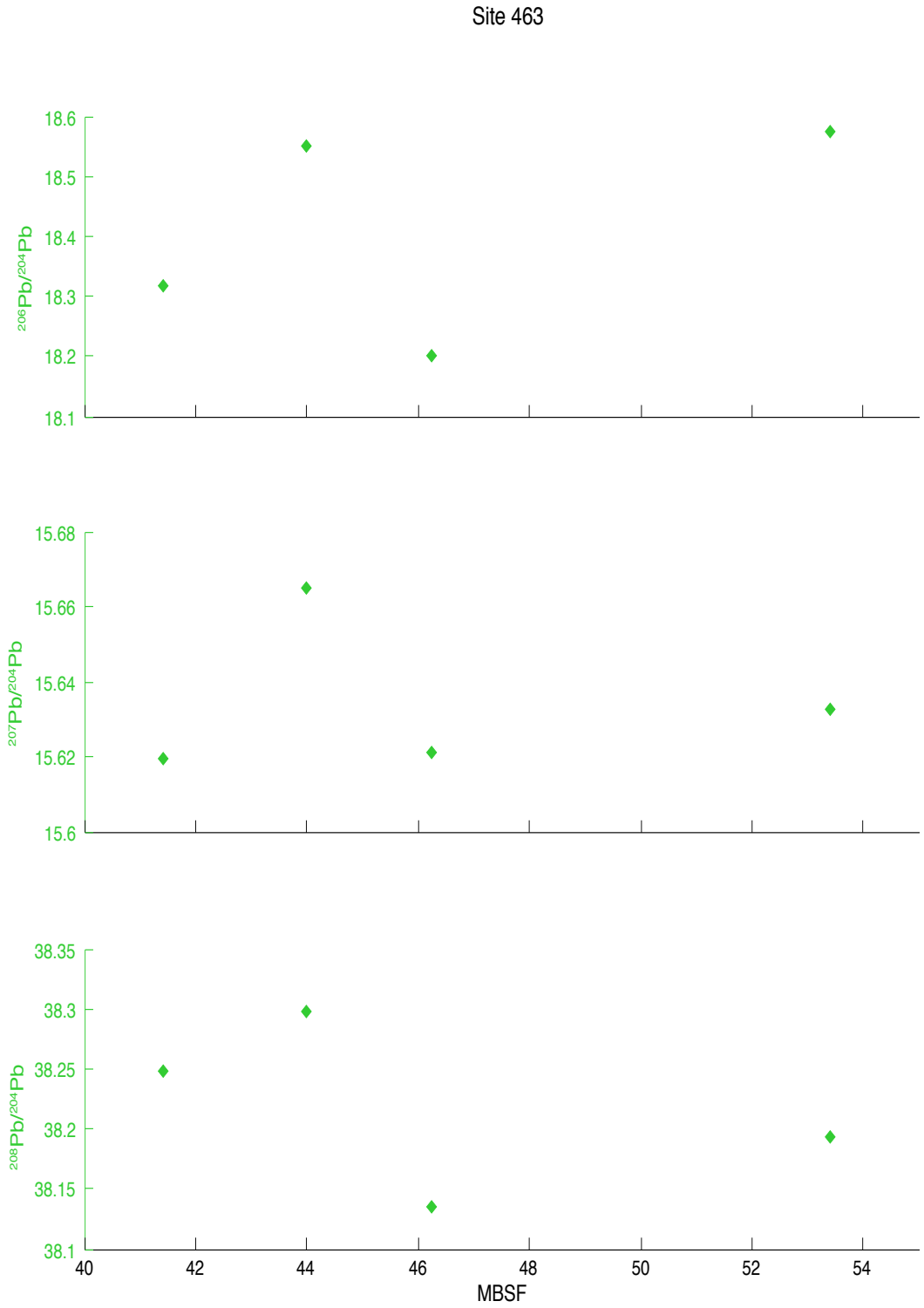

Figure 4.4 Pb isotopic data generated from Site 463.

4.5 Site 596- Paleolatitude 38°S, Paleodepth 5000 m

Site 596 (Fig. 4.5) seawater $^{206}Pb/^{204}Pb$ values increase from 18.96 to 19.0 over the interval 23.83 to 22.82 mbsf, then decrease to 18.9 at 21.37 mbsf and increase to 19.2 at 20.37 through 19.98 mbsf. Values decrease to 18.8 at 19.47 mbsf, then increase gradually to 18.9 at 18.73 mbsf and decrease to 18.8 at 18.41 mbsf. Values remain constant at 18.9 over the interval 18.01 to 16.25 mbsf, then increase to 19.3 at 14.88 mbsf, before they decrease to 18.8 at 14.65 mbsf and remain constant through 13.5 mbsf. The corresponding $^{207}Pb/^{204}Pb$ values decrease from 15.70 to 15.68 over the interval 23.83 to 22.82, then increase gradually to 15.78 at 20.37 mbsf. Values then decrease to 15.64 at 19.47 mbsf and increase gradually to 15.76 at 18.73 mbsf, then decrease gradually to 15.66 at 18.01 mbsf. Values then return to 15.76 at 17.92 through 16.74 mbsf, decrease to 15.67 at 16.25 mbsf, then increase to 15.80 at 14.88 mbsf, and then decrease to 15.71 at 14.65 through 13.5 mbsf. The $^{208}Pb/^{204}Pb$ values are constant at 38.8 over the interval 23.83 to 22.82, then generally increase to 39.0 at 20.37 mbsf, decrease to 38.7 at 19.98 mbsf and remain constant through 19.47 mbsf. Values increase gradually to 39.1 at 18.73 mbsf, decrease gradually back to 38.7 at 18.01 mbsf, then increase to 39.1 and remain constant over the interval 17.92 to 16.74 mbsf, decrease to 38.7 at 16.25 mbsf, then increase to 39.0 at 14.88 through 13.5 mbsf.

We analyzed the detrital Pb isotopic composition of two samples at Site 596. The values at 18.73 mbsf were 18.9, 15.64, and 38.8 for the $^{206}Pb/^{204}Pb$, $^{207}Pb/^{204}Pb$, and $^{208}Pb/^{204}Pb$ values respectively. The values at 17.92 mbsf were 18.9, 15.64, and 38.8 for the $^{206}Pb/^{204}Pb$, $^{207}Pb/^{204}Pb$, and $^{208}Pb/^{204}Pb$ values respectively.

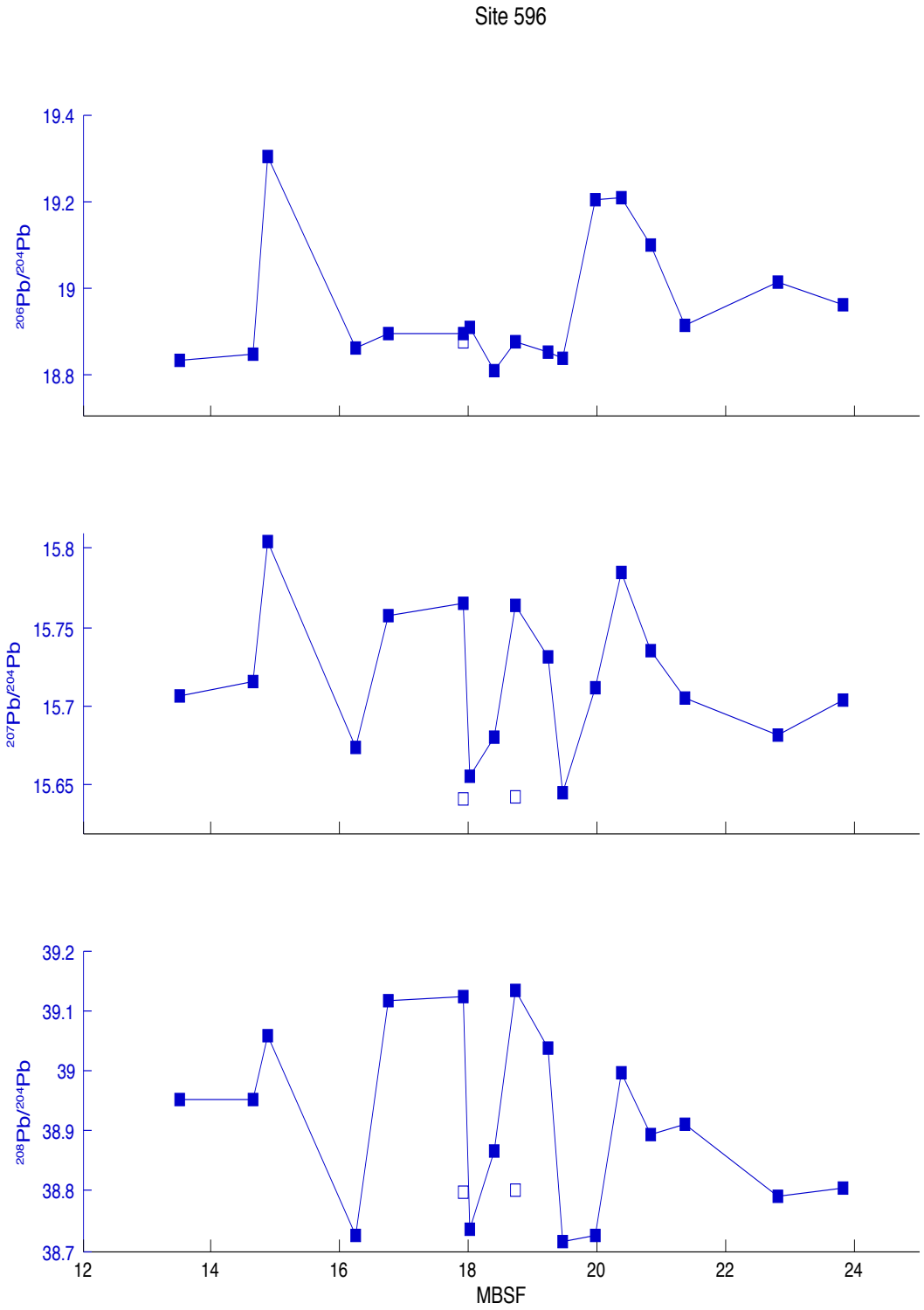

Figure 4.5 Pb isotopic data generated from Site 596. Open symbols represent detrital Pb values.

4.6 Site 323- Paleolatitude 65°S, Paleodepth 4000 m

Site 323 (Fig. 4.6) seawater $^{206}Pb/^{204}Pb$ values decrease gradually from 18.81 to 18.68 over the interval 698.39 to 682.85 mbsf, then increase gradually to 18.79 through 659.4 mbsf, and decrease to 18.74 at 658.64 mbsf, and remain constant through 657.39 mbsf. Values then rise gradually to 18.79 at 638.71, and decrease to 18.77 at 638.57. Repeated runs at 638.1 mbsf yield values of 18.69 and 18.73. The corresponding $^{207}Pb/^{204}Pb$ values decrease from 15.70 to 15.60 over the interval 698.39 to 682.85 mbsf, then increase to 15.67 at 660.14, decrease gradually to 15.63 at 657.84 mbsf, and increase gradually to 15.66 at 656.46. Values then decrease and remain constant at 15.65 over the interval 638.71 to 638.57, and repeated runs at 638.1 yield values of 15.63 and 15.67. The $^{208}Pb/^{204}Pb$ values decrease from 38.8 to 38.5 over the interval 698.39 to 682.85 mbsf, then increase gradually to 38.7 at 659.4, then remain at 38.6 and 38.6 over the interval 659.64 to 657.39 mbsf. Values increase gradually to 38.7 at 638.71 and remain constant through 638.57. Repeated runs at 638.1 mbsf yield values of 38.6 and 38.8.

We analyzed the detrital Pb isotopic composition of two samples at Site 596. The values at 664.72 mbsf were 18.8, 15.60, and 38.5 for the $^{206}Pb/^{204}Pb$, $^{207}Pb/^{204}Pb$, and $^{208}Pb/^{204}Pb$ values respectively. The values at 638.10 mbsf were 18.8, 15.63, and 38.7 for the $^{206}Pb/^{204}Pb$, $^{207}Pb/^{204}Pb$, and $^{208}Pb/^{204}Pb$ values respectively.

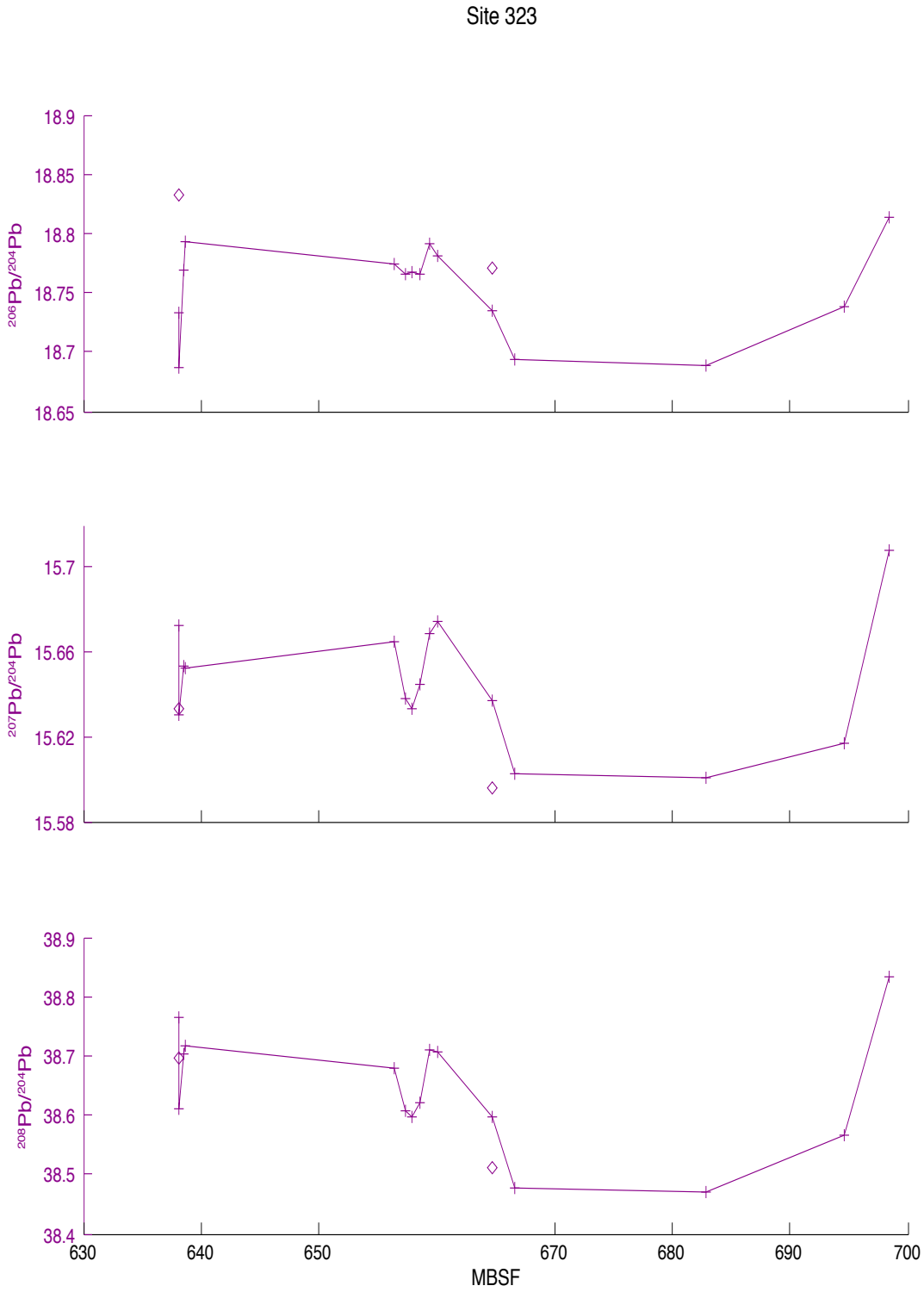

Figure 4.6 Pb isotopic data generated from Site 323. Open symbols represent detrital Pb values.

5. DISCUSSION

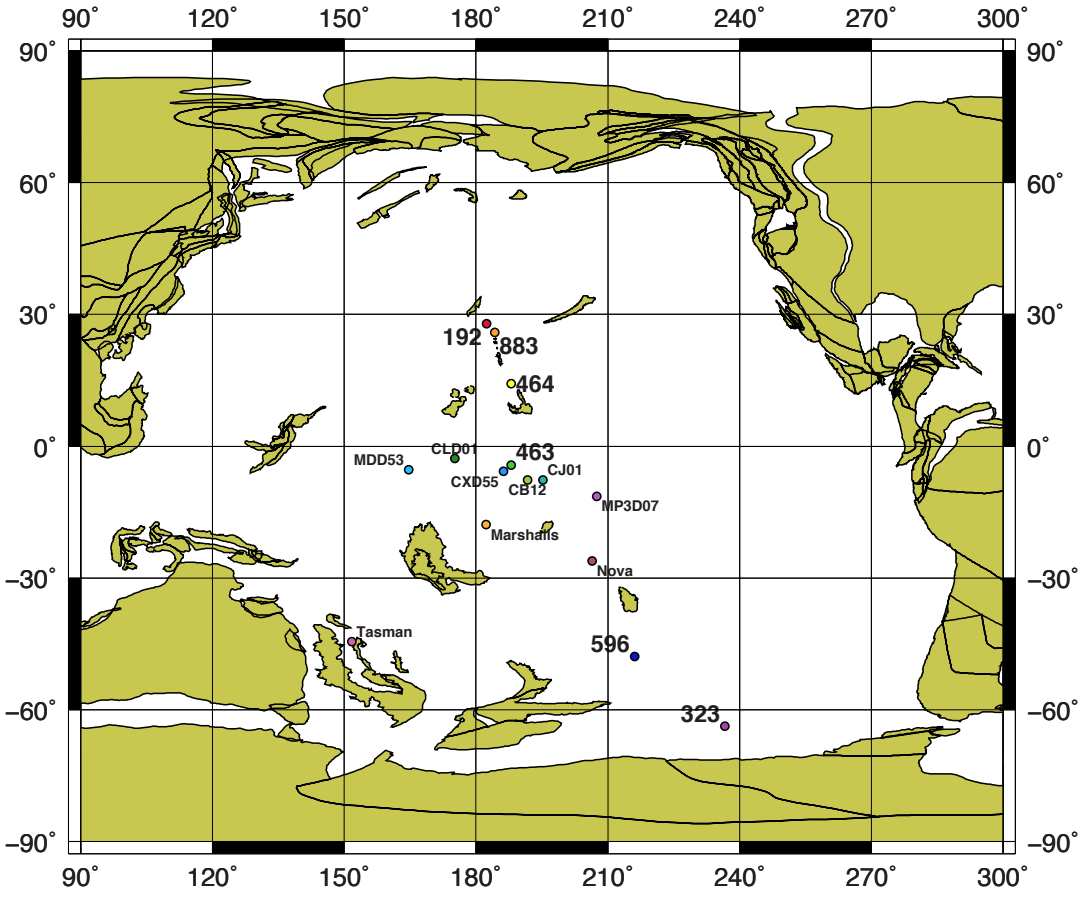

Figure 5.1 Plate tectonic reconstruction of Pacific 65 Ma. Tectonic configurations and locations of the study sites as well as locations of studied Fe-Mn crusts [*Chen et al.*, 2013; *Ling et al.*, 2005; *van de Flierdt et al.*, 2004] are also shown. This map was generated using the Ocean Drilling Stratigraphic Network (http://www.odsn.de/).

The $^{206}Pb/^{204}Pb$, $^{207}Pb/^{204}Pb$, and $^{208}Pb/^{204}Pb$ isotope values recorded by the Fe-Mn oxyhydroxide coatings of bulk sediment samples reflect the composition of Pb dissolved in contemporaneous seawater at the seafloor [*Abouchami et al.*, 1997; *Basak et al.*, 2011; *O'Nions et al.*, 1978]. The composition of dissolved Pb in seawater is

primarily influenced by local riverine inputs as well as dissolved eolian inputs [*Duce et al.*, 1991; *Frank*, 2002; *Henderson and Maier-Reimer*, 2002; *Jones et al.*, 2000]. The temporal variations in seawater $^{206,207,208}Pb/^{204}Pb$ recorded by Fe-Mn oxide minerals at a given location should reflect temporal variations in dissolved Pb advected into the study region, variations in contributions from dust input, as well as changes in local and regional weathering inputs.

The overall range of $^{206,207,208}Pb/^{204}Pb$ values recorded by the Fe-Mn oxide minerals in the six drill sites is consistent with previously published Pacific Fe-Mn crust values (Fig. 5.1, 5.2), although the minimum and maximum values recorded at the drill sites exceed the range of existing crust data. The greater range in seawater composition may reflect geography – the previously published crust data all derive from the tropical and subtropical Pacific, whereas the drill sites extend further to the north and south within the Pacific basin.

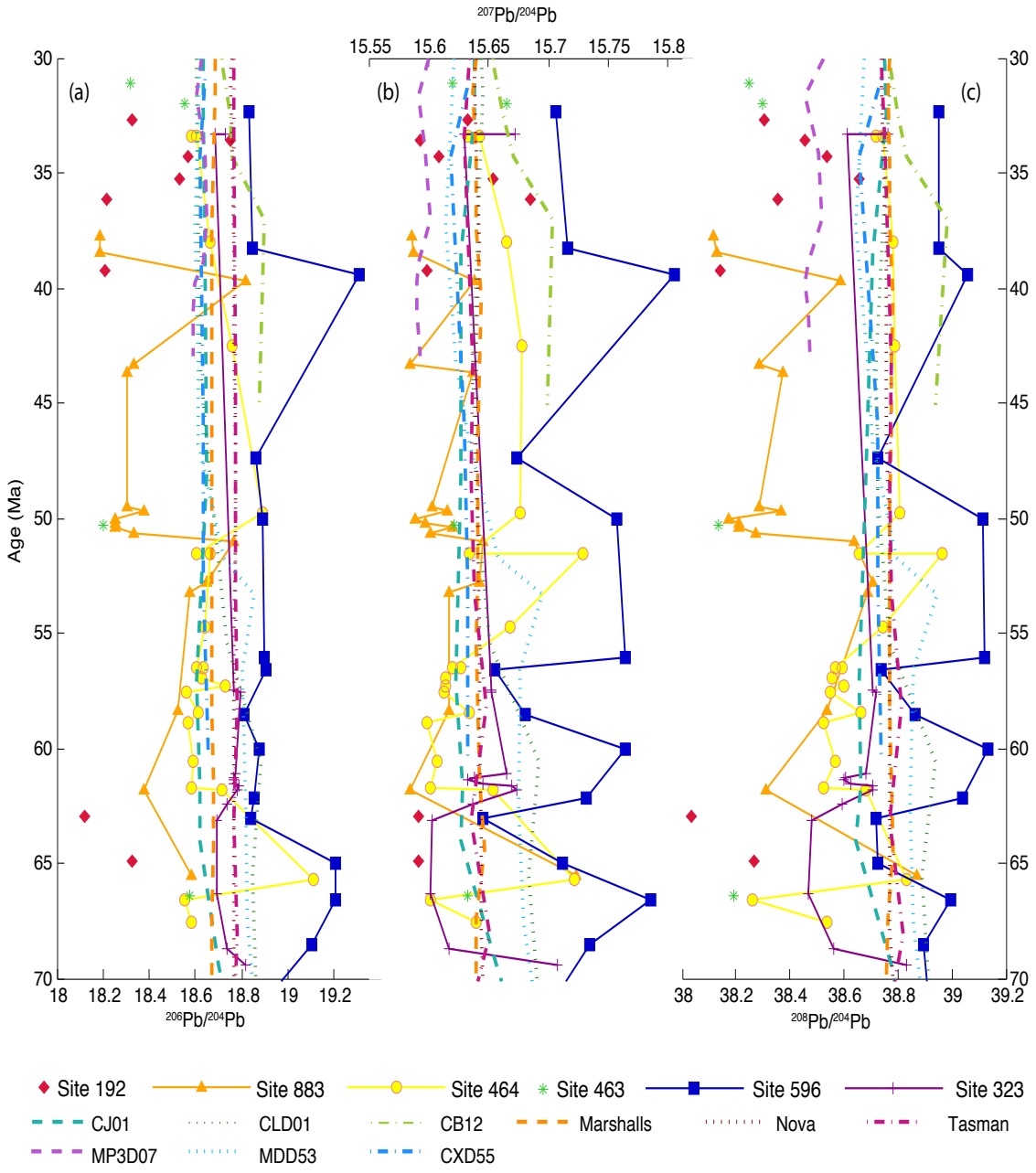

Figure 5.2 Comparison between data recovered from this study and published records: (a). $^{206}Pb/^{204}Pb$, (b). $^{207}Pb/^{204}Pb$, and (c). $^{208}Pb/^{204}Pb$. Previously published data includes Fe-Mn crusts from equatorial Pacific, D137-01 ("Nova"), and D27 2-1 ("Marshalls"), and southwest Pacific, 63KD ("Tasman") [*van de Flierdt et al.*, 2004], central north Pacific Fe-Mn crusts CJ01, CLD01, and CB12 [*Ling et al.*, 2005], and Fe-Mn crusts from western Pacific seamounts MDD53, central North Pacific seamounts CXD55 and MP3D07 [*Chen et al.*, 2013].

In general, the available data suggest that northern Pacific sites recorded relatively low Pb isotope values and southern sites recorded higher compositions (Fig. 5.3). Although it is difficult to directly compare North Pacific Sites 192 and 883 (water depths 2500 and 2000 m, respectively) due to the stratigraphic limitations of Site 192, the portions of the records with overlapping temporal coverage indicate similar values in all three Pb isotope systems. But the geographic relationship with seawater Pb isotopic composition seems to break down when we consider the rest of the sites to the south. For example, DSDP Site 464 (water depth 4000 m) in the northern subtropical Pacific is geographically closer to Sites 192 and 883, however the trends and values recorded at Site 464 more closely resemble those of southern DSDP Sites 323 and 596 (water depth 4000 and 5000 m, respectively). Furthermore, the available data from tropical Pacific DSDP Site 463 (water depth 2000 m) indicate relatively low Pb isotopic values more consistent with a "northern" type value.

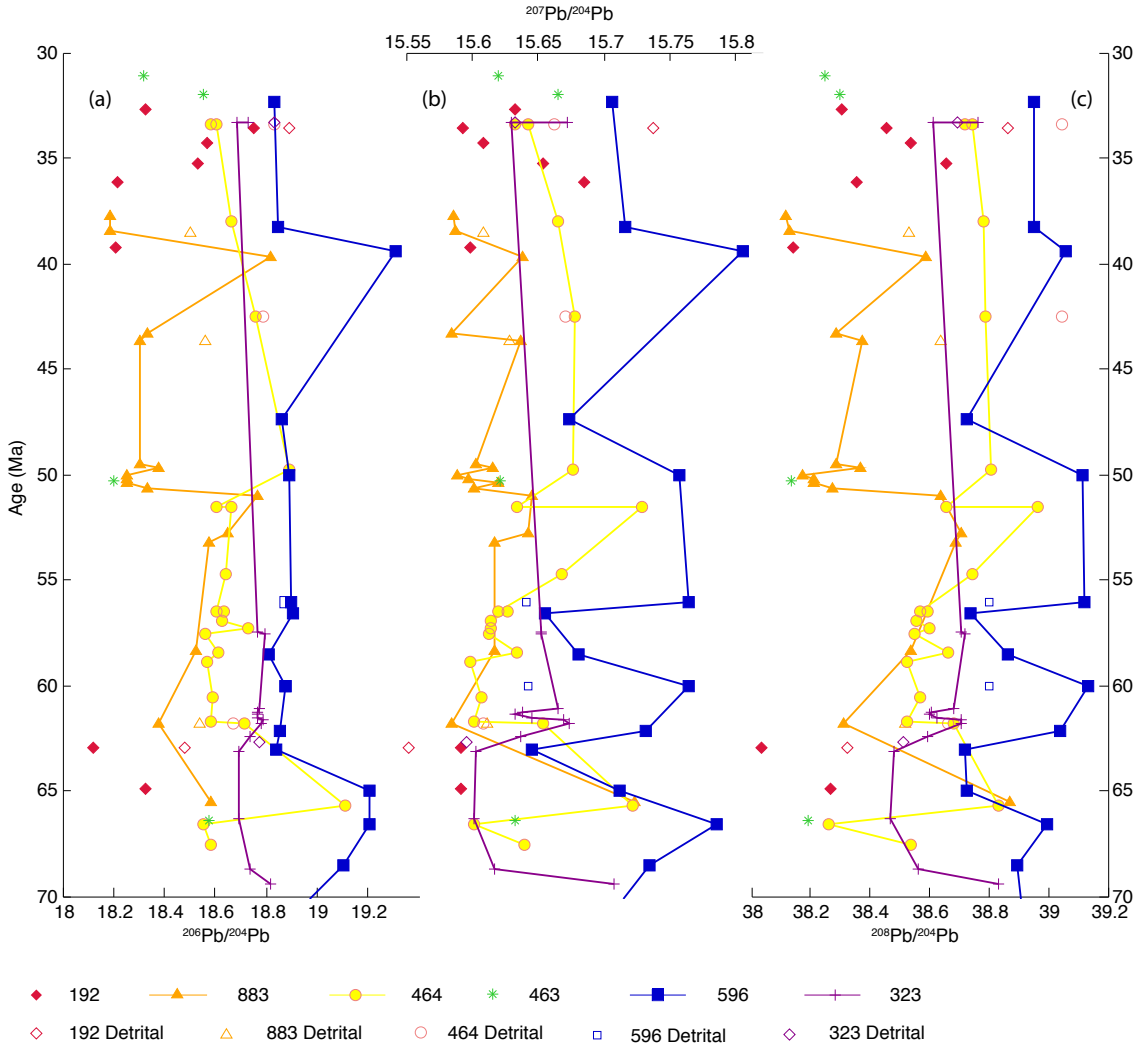

Figure 5.3 Overall comparison of seawater and detrital Pb isotopic time series from all study sites. (a). $^{206}Pb/^{204}Pb$, (b). $^{207}Pb/^{204}Pb$, and (c). $^{208}Pb/^{204}Pb$.

Variations in the three Pb isotope systems reflect different weathering sources [*Abouchami and Galer*, 1998; *Basak and Martin*, 2013; *van de Flierdt et al.*, 2003]. Basak & Martin [2013] demonstrated that seawater $^{207,208}Pb/^{204}Pb$ reflect weathering of silicate rocks, while those of $^{206}Pb/^{204}Pb$ reflect weathered ancient marine carbonates. The three Pb isotope ratios recorded at North Pacific Sites 192 and 883 tend to fluctuate

consistently, with generally coincident maxima and minima in each of the three tracers. The coincident variations in all three Pb systems might track the overall variations in dissolved Pb in the deep-water formation region. At Site 464, all three Pb isotope systems behave similarly with the exception of a transient increase recorded in $^{207,208}Pb/^{204}Pb$ values between ~56 and 51 Ma that is not apparent in the $^{206}Pb/^{204}Pb$ values. One potential explanation for the variations in $^{207,208}Pb/^{204}Pb$ without concomitant changes in $^{206}Pb/^{204}Pb$ is the contribution of Pb from the dissolution of detrital silicate dust. The hiatuses at Site 463 preclude significant evaluation of the covariation of the three Pb systems.

At South Pacific Site 596, all three isotopes record maxima at ~66 and 40 Ma, while $^{207,208}Pb/^{204}Pb$ values show additional peaks at ~60 and from ~56 to 50 Ma that do not occur in the $^{206}Pb/^{204}Pb$. These differences could be attributed to the same processes noted above for Site 464 – dissolution of silicate dust could have produced the increases in $^{207,208}Pb/^{204}Pb$ without impacting the corresponding $^{206}Pb/^{204}Pb$ values. At Site 323, all three isotope systems generally vary consistently, however the fluctuation in $^{206}Pb/^{204}Pb$ values are significantly lower than those evident in the $^{207,208}Pb/^{204}Pb$ values.

Comparison of the dissolved Pb isotopic composition derived from the oxide fraction with that recorded by the detrital sediment fraction also constrains the sources of Pb to the study sites. In the North Pacific, at Site 192, the detrital Pb isotope values in samples from ~34 and 63 Ma, respectively, are 0.1 to 0.4 higher than the corresponding seawater values, (Fig. 5.3, Table 5.1). At Site 883, the detrital $^{206}Pb/^{204}Pb$ and $^{208}Pb/^{204}Pb$ values were 0.2 to 0.4 higher than their corresponding seawater values, while

the seawater and detrital $^{207}Pb/^{204}Pb$ were the same. At Site 464, the difference between detrital and seawater Pb isotope values increased up-section with similar detrital and seawater values recorded at ~42 and 62 Ma (except the seawater $^{208}Pb/^{204}Pb$ value was 0.3 lower than the detrital value in the ~42 Ma sample), but detrital values recorded at ~33 Ma were 0.2 to 0.3 higher than the associated seawater values. Two detrital samples from Site 596 (~56 and 60 Ma, respectively) record $^{206}Pb/^{204}Pb$ nearly identical to the seawater ratios. However, the corresponding seawater $^{207,208}Pb/^{204}Pb$ values were 0.1 to 0.3 higher. Site 323 detrital analyses (~33 and 63 Ma, respectively) approximately coincide with the contemporaneous seawater values (with maximum differences of 0.1).

The locations of Site 192, 464, 596 and 883 were relatively far from any ancient shoreline (Figure 5.1), thus fluvial or hemipelagic sources of Pb likely didn't contribute to the detrital signal recorded by the oxide fraction. Thus, the likely source of detrital Pb would have been dissolution of eolian dust from various sources. Pettke et al. [2002] suggest that prior to ~40 Ma North Pacific dust was a mixture of Caribbean volcanic ash [*Sigurdsson et al.*, 2000], and continental dust. The new Pb data suggest that dust inputs more strongly influenced the seawater Pb composition at Site 464 than the more northern Sites 192 and 883. The Pb data also indicate higher detrital than seawater values at North Pacific Sites 192, 464 and 883. Moreover, the detrital values of Site 192 ~63 Ma, and Site 883 ~62 Ma are close to the seawater composition of Site 464 at that time (Fig. 5.3), supporting a strong contribution of continental dust to the North Pacific.

The proximity of Site 323 to Antarctica, combined with the similarity of detrital and seawater Pb isotope values suggests that the Pb recorded at Site 323 derived from

Antarctic weathering inputs. The Pb isotope values recorded at Site 323 are consistent with values from terrains in the Antarctic Peninsula. $^{206}Pb/^{204}Pb$ values of basalts in this region are between 18.7 and 19.5, while $^{206}Pb/^{204}Pb$ values are between 15.53 and 15.68, and $^{208}Pb/^{204}Pb$ values are between 38.2 to 39.2 [*Finn et al.*, 2005; *Hole et al.*, 1993]. The relatively consistent values recorded throughout the study interval suggest that the composition of weathering inputs delivered to the region did not vary significantly.

Table 5.1 Comparison of detrital Pb isotopic data to corresponding seawater $^{206,207,208}Pb/^{204}Pb$ values. The nearest seawater values are provided for detrital analyses without corresponding seawater Pb values.

			Seawater			Detrital		
Sample ID	Depth (mbsf)	Age (Ma)	$^{206}Pb/^{204}Pb$	$^{207}Pb/^{204}Pb$	$^{208}Pb/^{204}Pb$	$^{206}Pb/^{204}Pb$	$^{207}Pb/^{204}Pb$	$^{208}Pb/^{204}Pb$
Site 192								
1-3, 51-53	945.51	33.54	18.7533	15.5928	38.4561	18.8939	15.7377	38.8641
4-2, 92-94	1020.42	62.94	18.1213	15.5922	38.0335	18.4837	15.5528	38.3258
Site 883								
77-1, 28-30	730.18	38.45	18.1860	15.5868	38.1279			
77-1, 31-33	731.21	38.55				18.5003	15.6083	38.5292
79-3, 65-67	753.15	43.70	18.3037	15.6367	38.3716	18.5623	15.6289	38.6385
86-5, 5-7	824.55	61.80	18.3776	15.5840	38.3087	18.5378	15.6116	38.5187
Site 464								
6-1, 90	42.40	33.42	18.5826	15.6323	38.7207	18.8287	15.6629	39.0469
6-1, 90	42.40	33.42	18.6018	15.6421	38.7422			
6-3, 100	45.50	42.55	18.7556	15.6785	38.7859	18.7907	15.6710	39.0484
8-2, 84	62.16	61.79	18.7113	15.6544	38.6791	18.6703	15.6089	38.6651
Site 596								
3-2, 132-134	17.92	56.10	18.8945	15.7646	39.1236	18.8757	15.6416	38.7987
3-3, 63-65	18.73	60.03	18.8766	15.7641	39.1340	18.8752	15.6429	38.8018
Site 323								
14-2 60-62	638.10	33.36	18.7324	15.6728	38.7659	18.8331	15.6330	38.6946
14-2 60-62	638.10	33.36	18.6869	15.6301	38.6110			
16-1, 22-24	664.72	62.72	18.7341	15.6375	38.5955	18.7712	15.5960	38.5124

Comparison of the Pacific seawater Pb isotope records with those of Nd isotopes may also help constrain the potential sources of dissolved Pb to the study regions. If the sole source of dissolved Pb to the Pacific were fluvial inputs into the convection regions then we would expect a clear north-south progression in the Pb isotope data. In other words, the Pb and Nd isotope patterns recorded at each site should be coupled. However, as noted before, no such geographic relationship exists in the Pb isotopic records of this study. This lack of apparent north-south variation in the deep-water Pb isotopic composition contrasts with seawater neodymium isotope records generated from the same set of drill sites and crusts. Nd isotope data indicate a clear north-south progression in water composition interpreted to reflect convection of waters in the North and South Pacific [*Hague et al.*, 2012; *Thomas*, 2004; *Thomas et al.*, in review]. The observation that seawater Pb isotope records do not exhibit the same trend suggests that the source(s) of dissolved Pb to the Pacific differed from those of Nd [*Erel et al.*, 1994; *Jones et al.*, 2000; *von Blanckenburg and Nägler*, 2001]. Here we explore the relationship between dissolved Nd and Pb at each site to evaluate the extent to which the sources were similar or different.

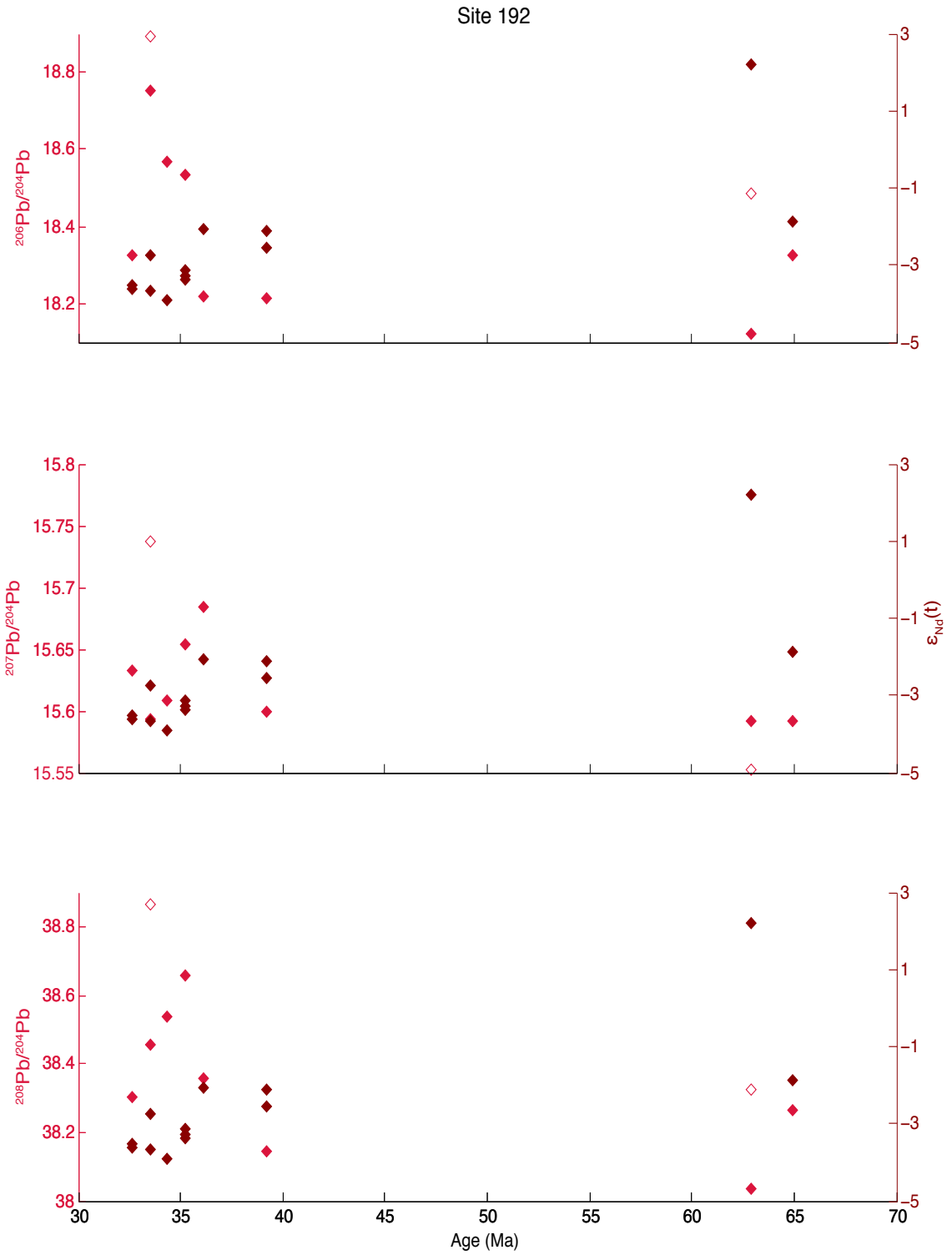

Figure 5.4 Time-series of Pb and Nd isotopic compositions at Site 192. Open symbols are representative of detrital Pb values. $\varepsilon_{Nd}(t)$ data at Site 192 was collected by Hague et al. [2012].

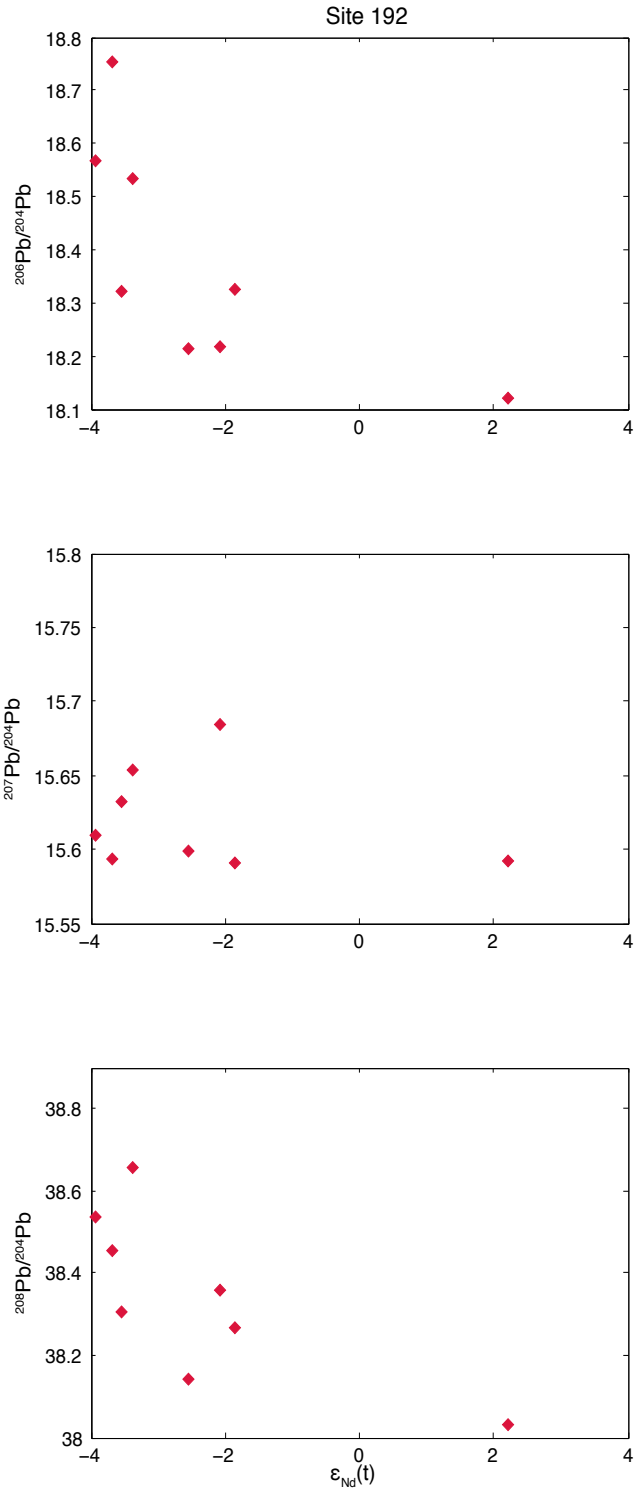

Figure 5.5 Comparative cross-plots of $^{206,207,208}Pb/^{204}Pb$ versus $\varepsilon_{Nd}(t)$ values at Site 192. $\varepsilon_{Nd}(t)$ data at Site 192 was collected by Hague et al. [2012].

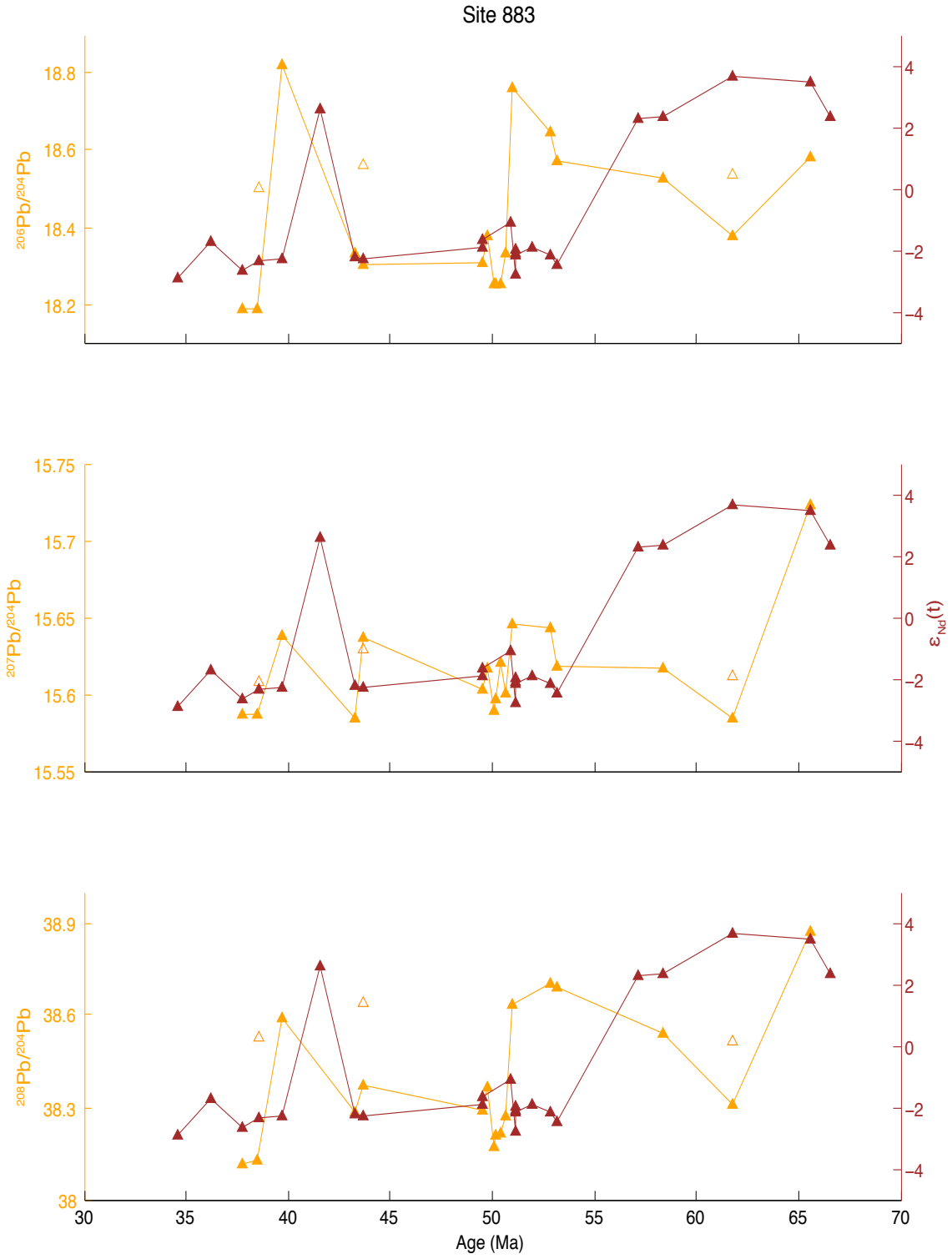

Figure 5.6 Time-series of Pb and Nd isotopic compositions at Site 883. Open symbols are representative of detrital Pb values. $\varepsilon_{Nd}(t)$ data at Site 883 was collected by Hague et al. [2012].

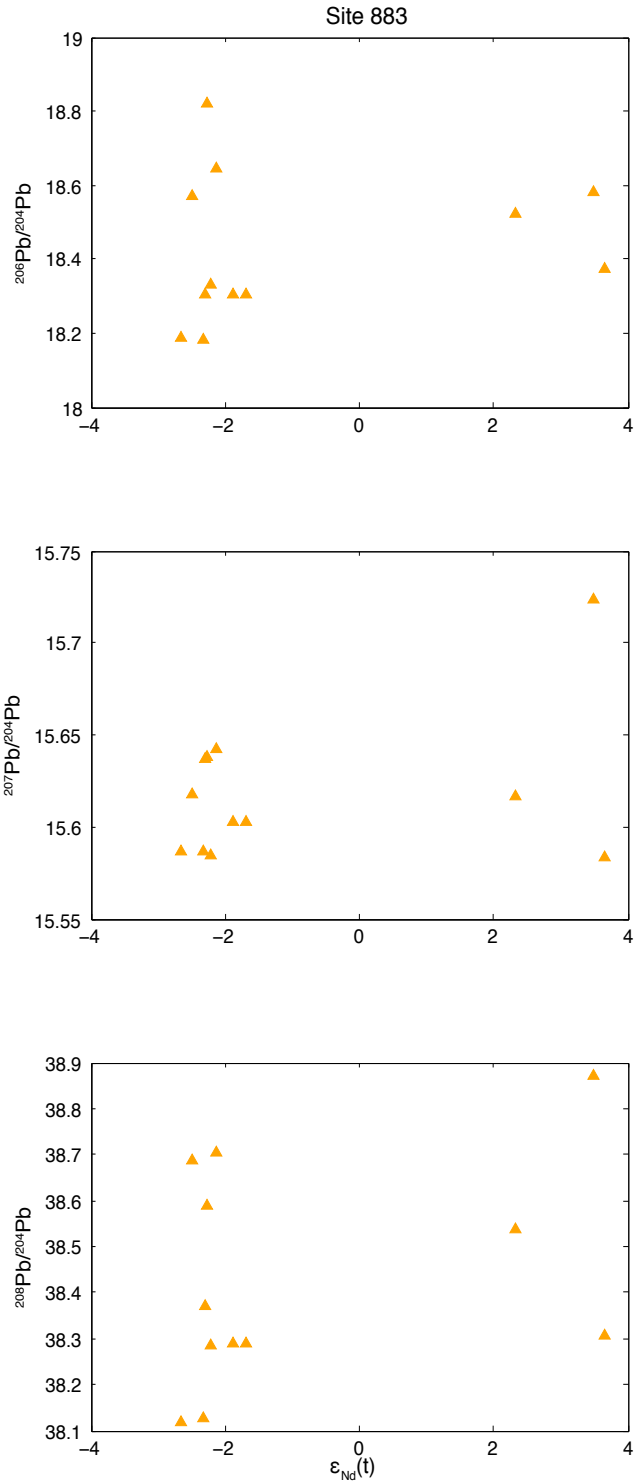

Figure 5.7 Comparative cross-plots of $^{206,207,208}Pb/^{204}Pb$ versus $\varepsilon_{Nd}(t)$ values at Site 883. $\varepsilon_{Nd}(t)$ data at Site 883 was collected by Hague et al. [2012].

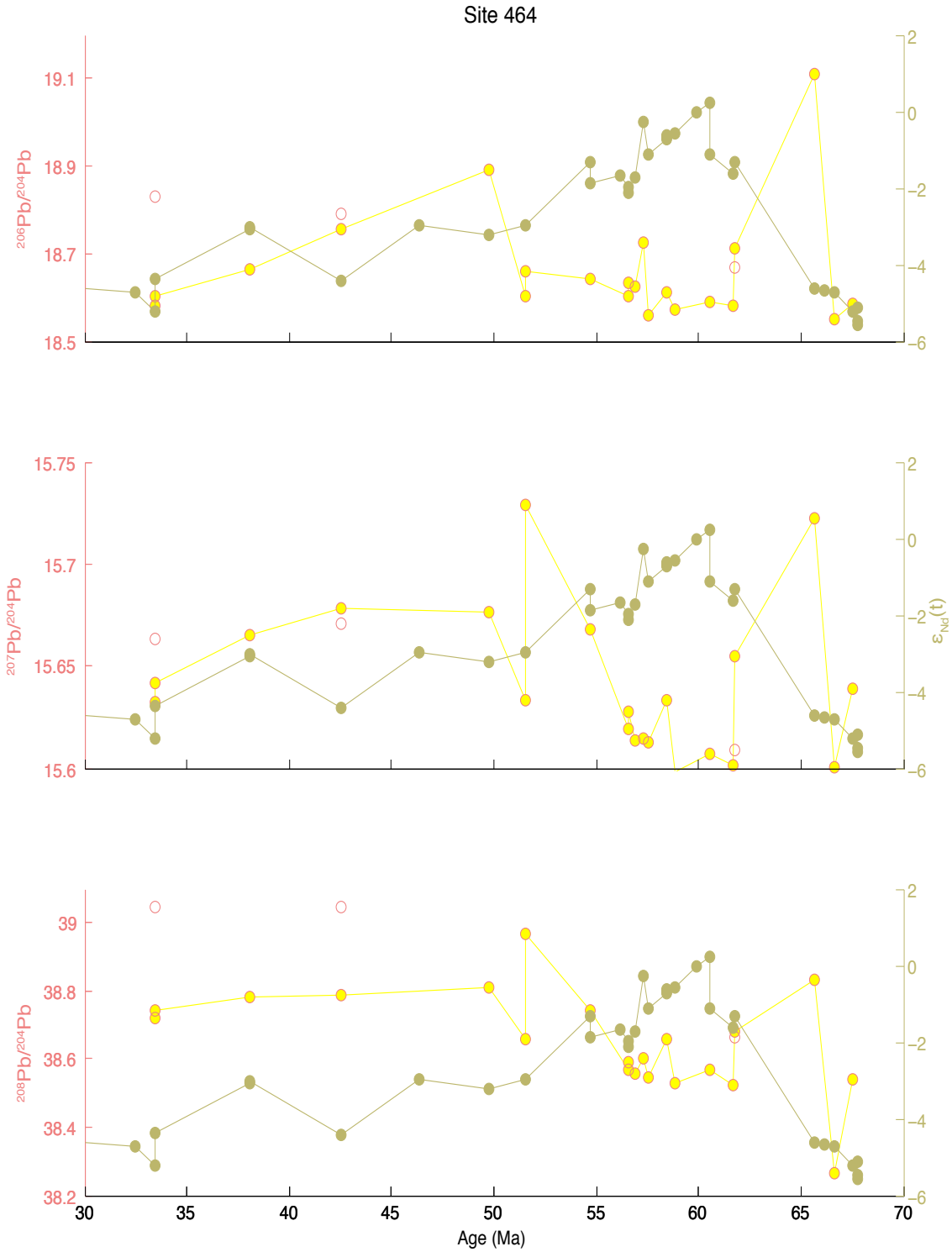

Figure 5.8 Time-series of Pb and Nd isotopic compositions at Site 464. Open symbols are representative of detrital Pb values. $\varepsilon_{Nd}(t)$ data at Site 464 was collected by Hague et al. [2012].

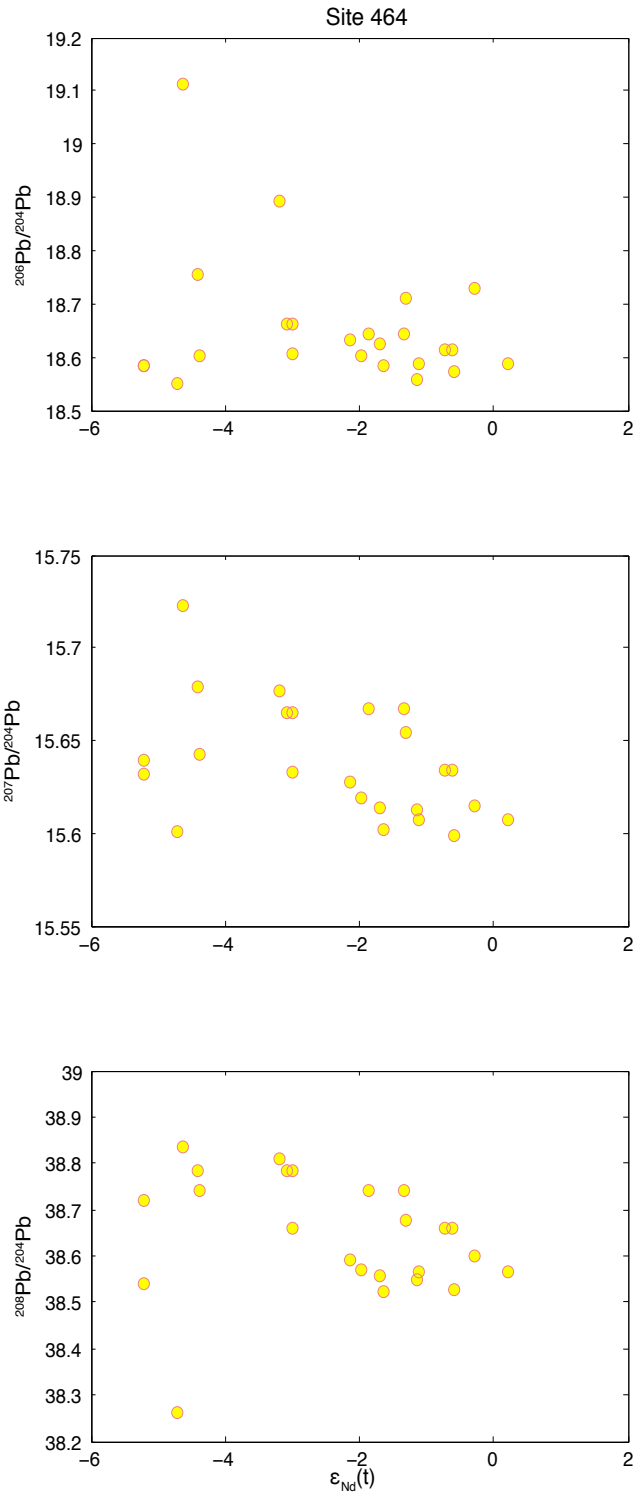

Figure 5.9 Comparative cross-plots of $^{206,207,208}Pb/^{204}Pb$ versus $\varepsilon_{Nd}(t)$ values at Site 464. $\varepsilon_{Nd}(t)$ data at Site 464 collected by Hague et al. [2012]

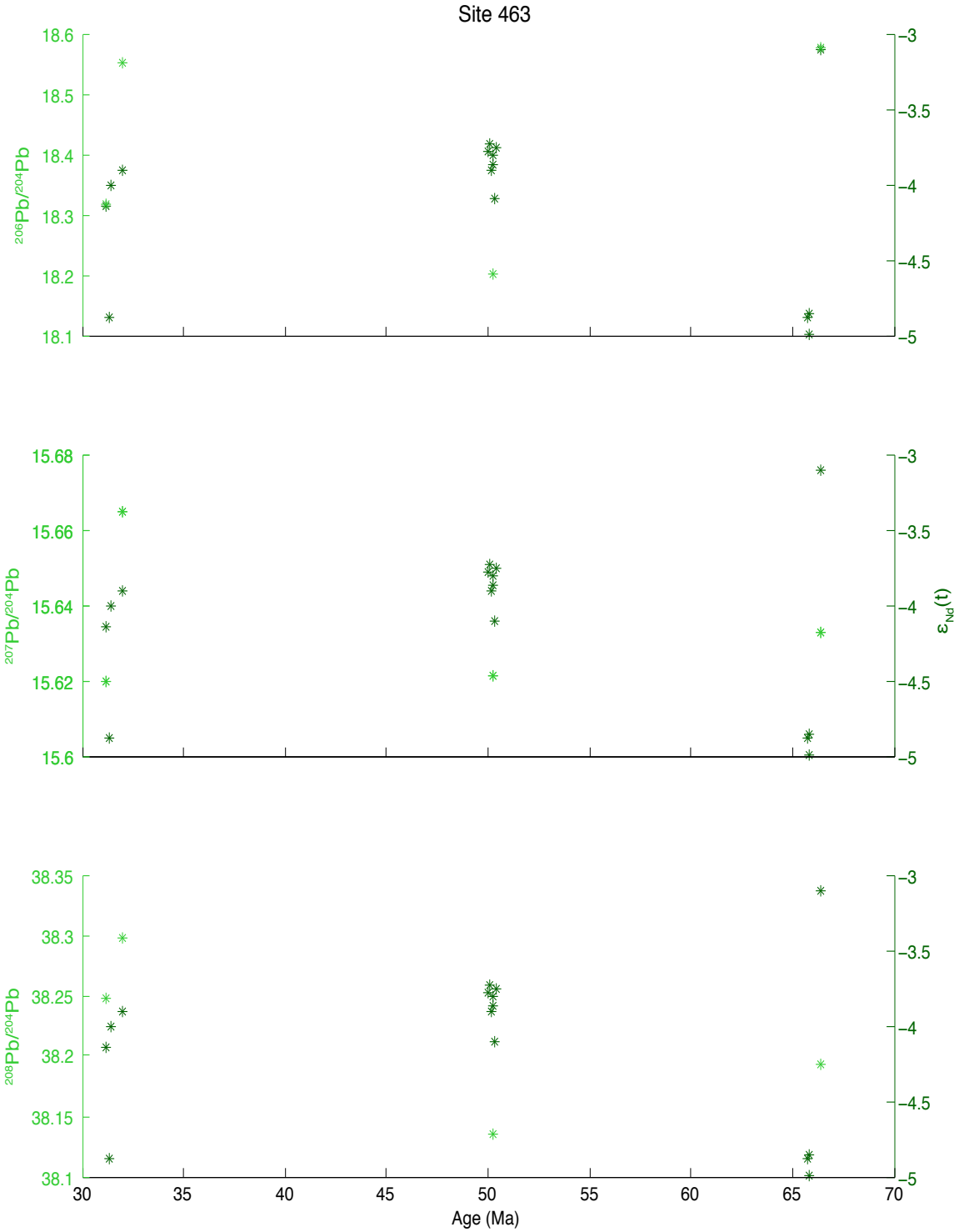

Figure 5.10 Time-series of Pb and Nd isotopic compositions at Site 463. $\varepsilon_{Nd}(t)$ data at Site 463 was collected by Thomas et al [in review].

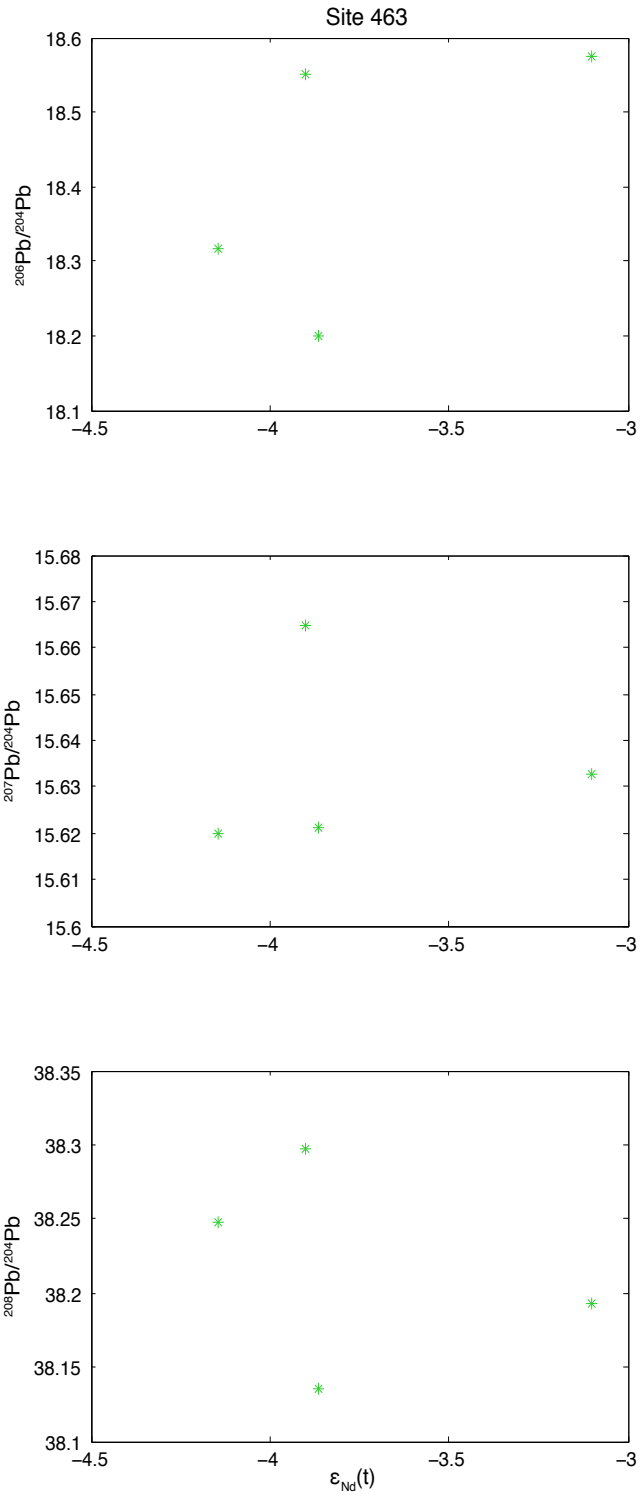

Figure 5.11 Comparative cross-plots of $^{206,207,208}Pb/^{204}Pb$ versus $\varepsilon_{Nd}(t)$ values at Site 463. $\varepsilon_{Nd}(t)$ data at Site 463 collected by Thomas et al. [in review]

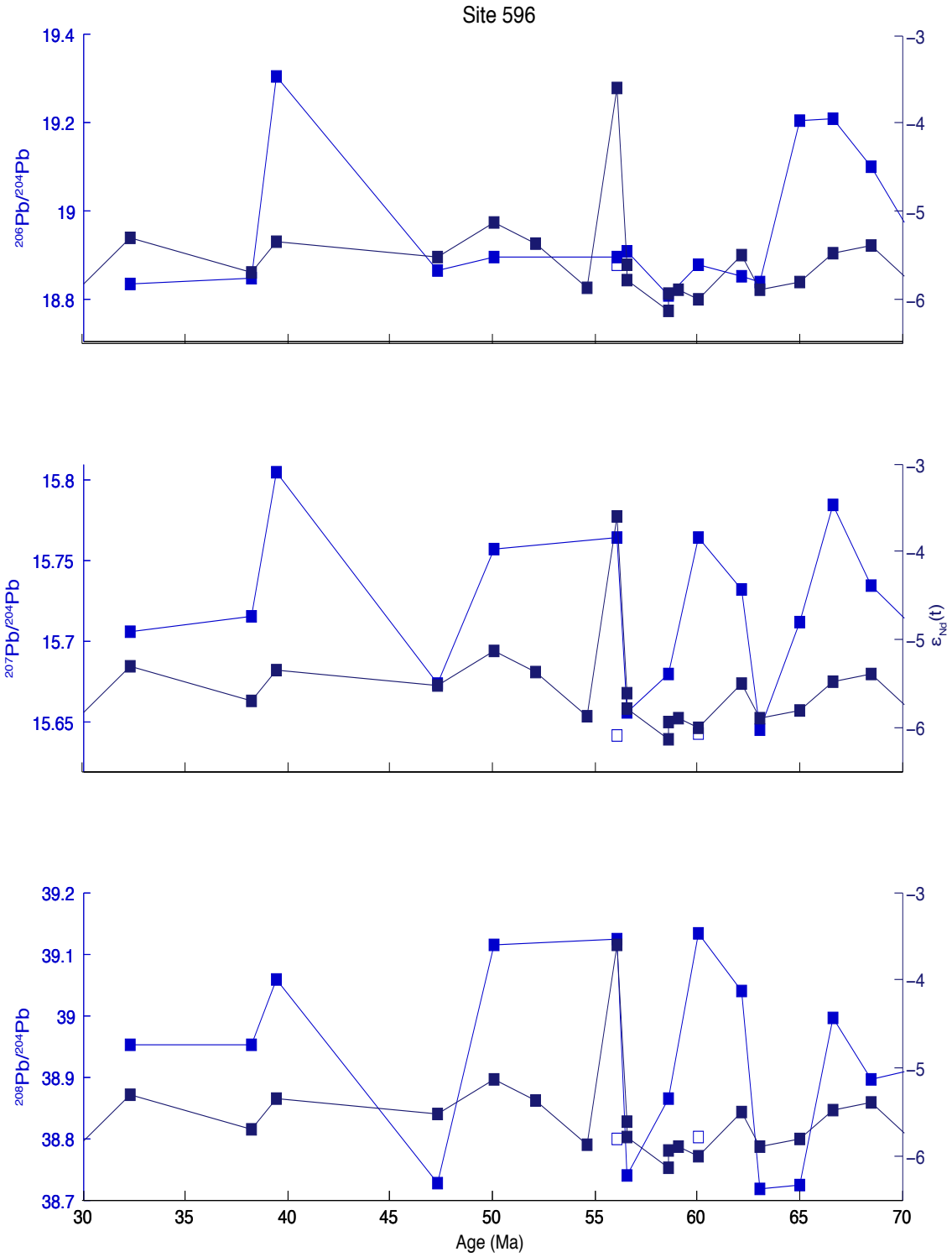

Figure 5.12 Time-series of Pb and Nd isotopic compositions at Site 596. Open symbols are representative of detrital Pb values. $\varepsilon_{Nd}(t)$ data at Site 596 was collected by Thomas et al, [in review].

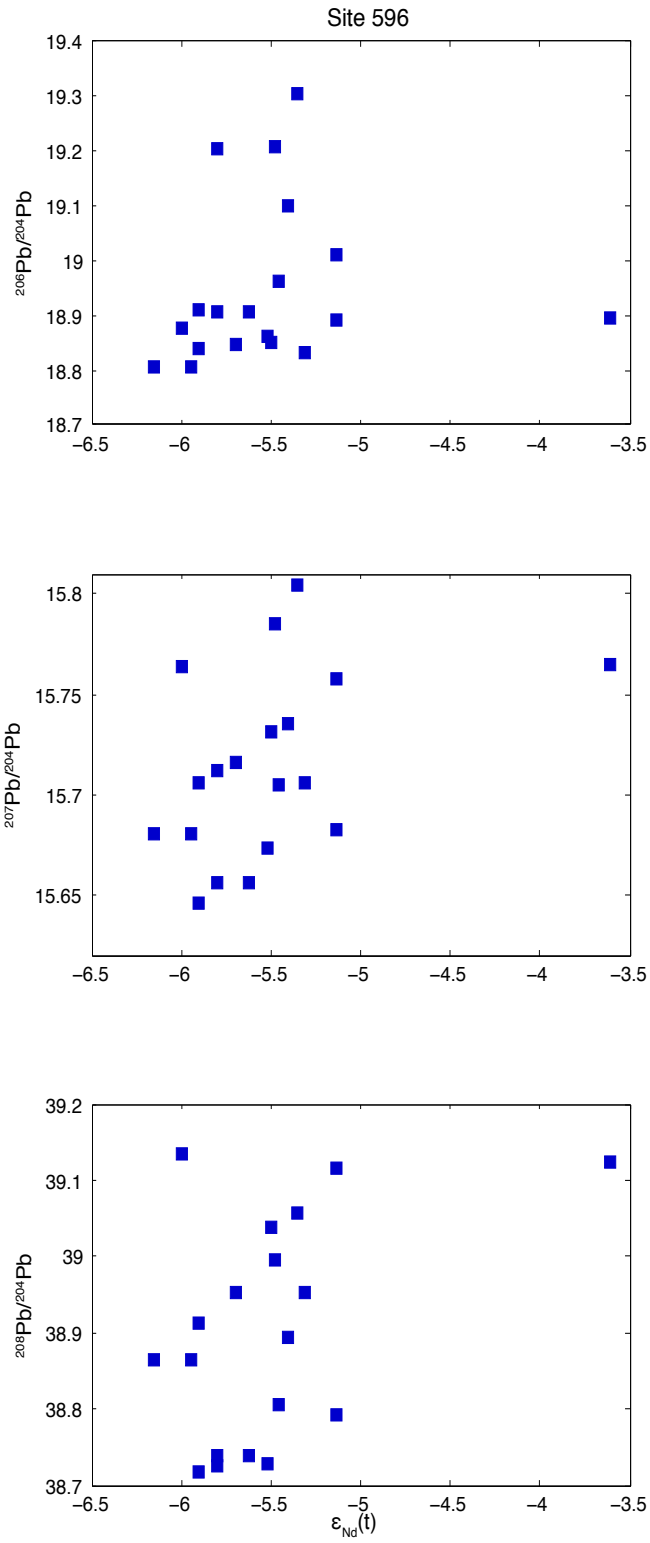

Figure 5.13 Comparative cross-plots of $^{206,207,208}Pb/^{204}Pb$ versus $\varepsilon_{Nd}(t)$ values at Site 596. $\varepsilon_{Nd}(t)$ data at Site 596 collected by Thomas et al. [in review].

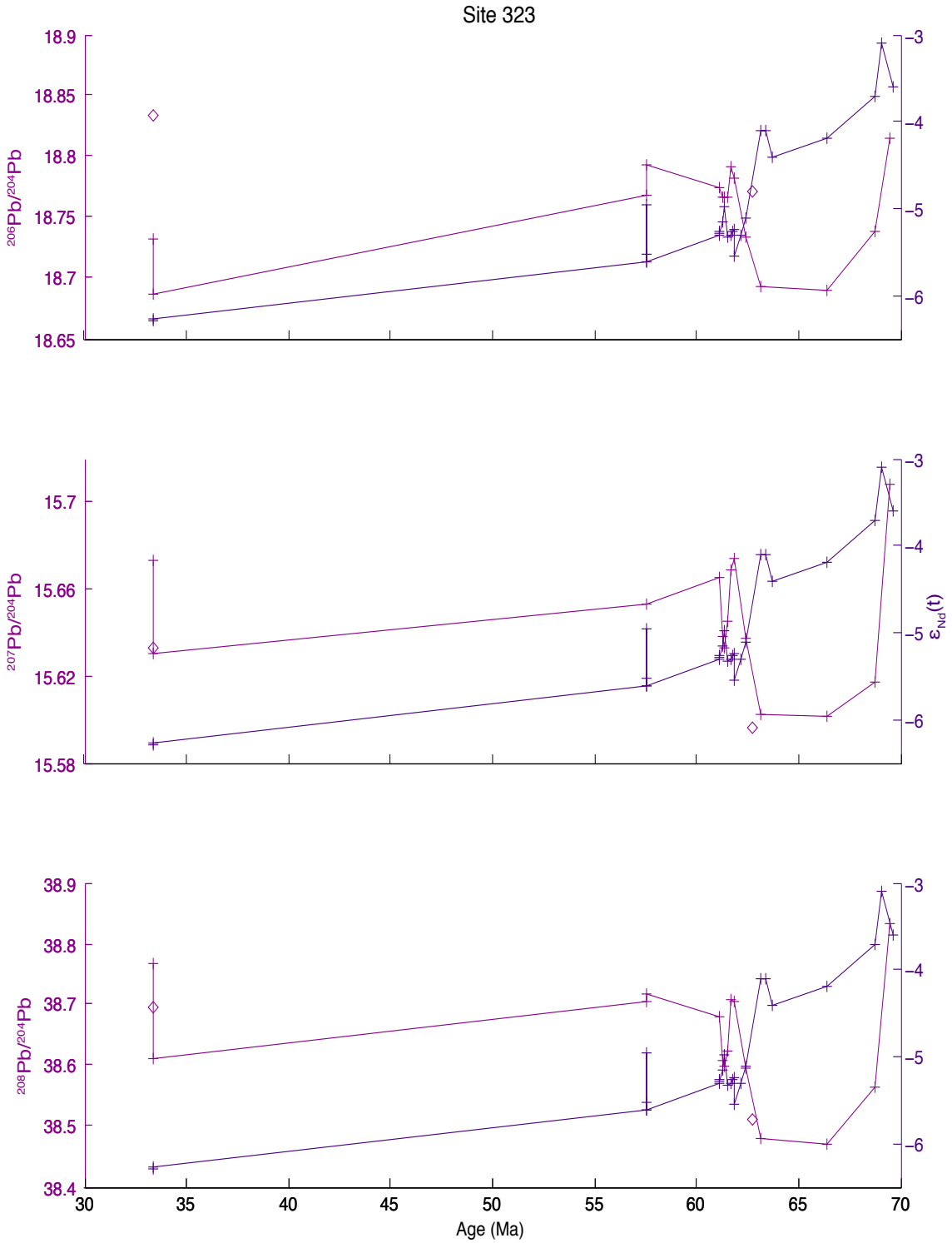

Figure 5.14 Time-series of Pb and Nd isotopic compositions at Site 323. Open symbols are representative of detrital Pb values. $\varepsilon_{Nd}(t)$ data at Site 323 was collected by Thomas et al, [in review].

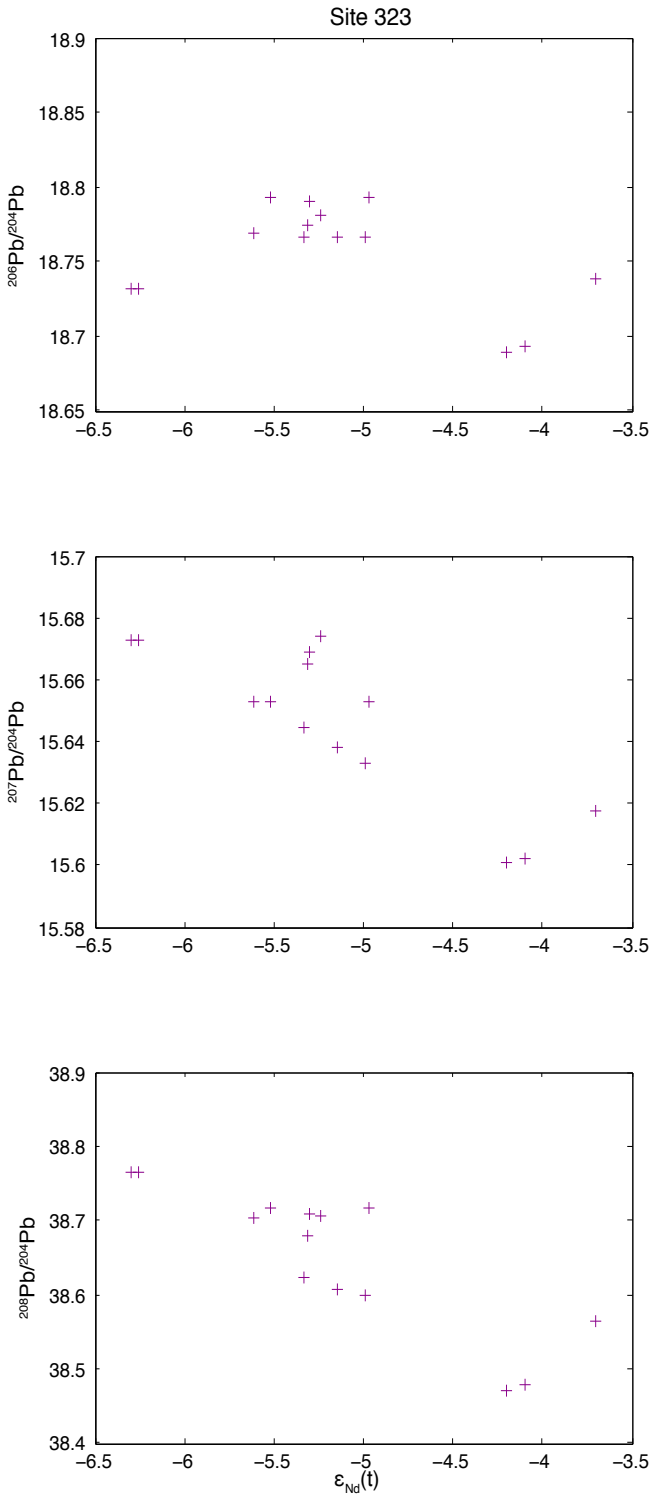

Figure 5.15 Comparative cross-plots of $^{206,207,208}Pb/^{204}Pb$ versus $\varepsilon_{Nd}(t)$ values at Site 323. $\varepsilon_{Nd}(t)$ data at Site 323 collected by Thomas et al. [in review].

Cross-plots of Pb versus Nd isotopes, as well as a direct comparison of the Pb and Nd isotope time series reveal several important features of the Pacific reconstruction (Fig. 5.4-5.15). At Site 192, direct comparison of the Nd and Pb time series indicates that shifts in the seawater Nd isotopic composition generally correspond to shifts in Pb, particularly in the $^{206,208}Pb/^{204}Pb$ records (Fig. 5.4). Pb isotope values show a weak inverse relationship to Nd isotope values, most apparent in the $^{206,208}Pb/^{204}Pb$ records (Fig. 5.5). These relationships suggest that the dissolved Nd and Pb at Site 192 may have been coupled, and thus most likely influenced by the composition of the water mass that advected into the study region. At Site 883 the time series suggests an inverse relationship from ~62 to 50 Ma in which the Pb isotopic composition decreases as Nd increases and vice versa (Fig. 5.6), however there is little apparent relationship between Pb and Nd in the cross-plots (Fig. 5.7). This relationship is consistent with the apparent coupling of Nd and Pb at nearby Site 192 and again suggests that both tracers likely were influenced by the water mass. The ocean island arcs in the North Pacific have $^{206}Pb/^{204}Pb$ ratios between ~17.9 and 18.7, $^{207}Pb/^{204}Pb$ ratios between ~15.4 and 15.7, and $^{208}Pb/^{204}Pb$ ratios between ~37.7 and 38.9 [*Sun*, 1980]. Pacific continental arcs have $^{206}Pb/^{204}Pb$ ratios between 17.9 and 19.4, $^{207}Pb/^{204}Pb$ between ~15.52 to 15.68, and $^{208}Pb/^{204}Pb$ ratios between ~38.3 to 39.1 [*von Blanckenburg et al.*, 1996]. The Pb isotopic composition at Sites 192 and 883 falls well within these ranges, however, the large amount of overlap in Pb ratios for each source makes it difficult to determine provenance.

Site 464, located further to the south of Sites 192 and 883, demonstrated a similar pattern in which there is no clear relationship between Pb and Nd in cross-plot but general inverse trends in the time series (Fig. 5.8, 5.9). For example, maximum Nd isotope values recorded between ~61 to 50 Ma correspond with relatively low Pb isotope values in all three systems. In fact, the Pb and Nd values from ~66 to 50 Ma show an inverse relationship, much like that in Sites 192 and 883. After ~50 Ma, Pb and Nd tend to co-vary (e.g., Nd and Pb both decrease to the top of the study interval). This change in the relationship between Nd and Pb could reflect a change in the dominant source of dissolved Pb to the central North Pacific region. From ~61 to 50 Ma, the dissolved Pb composition was likely controlled by water mass composition. This is consistent with Nd isotope evidence for a strong contribution of North Pacific Deep Water (NPDW) to the region over the time period [*Hague et al.*, 2012]. Subsequently, as convection of NPDW waned and the contribution of deep waters from the South Pacific increased (SPDW), the Nd isotope composition decreased. However the Pb isotope composition also decreased suggesting that the two tracers decoupled. One explanation for the decoupling could involve the more distal source of South Pacific deep waters – because Pb has a much shorter residence time than Nd, a water mass sourced from the South Pacific might lose its Pb signature by the time it reached the central North Pacific. Thus dust dissolution could have impacted the dissolved Pb composition of the deep waters more. The range of Pb isotopes at Site 464 is mostly in agreement with the previously discussed potential sources, but the overlapping ranges of their Pb ratios makes it

difficult to determine if there truly was a change from weathering inputs into the NPDW source region to dissolution of dust and ash above ~50 Ma.

The presence of two substantial hiatuses at Site 463 in the tropical central Pacific preclude any meaningful comparison between the existing Pb and Nd isotope values (Fig. 5.10, 5.11). The Pb isotopic composition at this site is more consistent with the values found in North Pacific sites (Fig. 5.3).

Comparison of the Pb and Nd isotope ratios recorded ay Site 596 suggests that the two isotope systems were not coupled (Fig. 5.12, 5.13). The Nd isotope values (with the exception of one radiogenic analysis at ~56 Ma) were nearly constant throughout the study interval, in contrast to the variable Pb isotope values recorded in all three Pb isotope systems. The most likely explanation for these differing patterns is that the water mass composition dominated the Nd signature while the Pb isotopic composition was influenced by dust or ash dissolution. The high amount of variability in Pb isotopes at Site 596, especially $^{207,208}Pb/^{204}Pb$, suggests more than one source contributed to the isotopic composition in this region. Some potential Pb sources to the subtropical South Pacific may include Australia and New Zealand that may have been transported through the Southwest Pacific [*Nakai et al.*, 1993]. The South American Andes might also have provided some influence to Pacific Pb. Central Andes $^{206}Pb/^{204}Pb$ concentrations fall between ~17.2 and 18.8, $^{207}Pb/^{204}Pb$ between ~15.6 and 15.73, and $^{208}Pb/^{204}Pb$ between ~36.9 and 39.1 [*Egenhoff and Lucassen*, 2003]. However, it is unlikely that both sources of dust are represented at the same location. The location of Site 596 during the time period would most likely have had inputs from westerly winds.

At Site 323, a direct comparison of the Nd and Pb time series suggests Pb and Nd were coupled (Fig. 5.14). Cross-plots of Pb versus Nd show a moderate inverse relationship throughout the record, particularly in the $^{207,208}Pb/^{204}Pb$ records (Fig. 5.15), indicating the Pb composition may have been influenced by advected water masses into the study region. The proximity of Site 323 to potential sources in Antarctica makes this a likely scenario. The range of Pb values at Site 323 are in agreement with the lower end-member values of basalts from the Antarctic Peninsula, with typical $^{206}Pb/^{204}Pb$ ratios between ~18.7 and 19.5, $^{207}Pb/^{204}Pb$ ratios between ~15.53 and 15.68, and $^{208}Pb/^{204}Pb$ ratios between ~38.2 to 39.2 [*Finn et al.*, 2005; *Hole et al.*, 1993]. Pb values from Marie Byrd Land and other West Antarctic tills however, are too high to be plausible sources ($^{206}Pb/^{204}Pb$ ratios between 19.5 and 21, $^{207}Pb/^{204}Pb$ ratios between 15.6 and 15.75, and $^{208}Pb/^{204}Pb$ ratios between 38.75 and 40.25) [*Finn et al.*, 2005; *Lang Farmer et al.*, 2006].

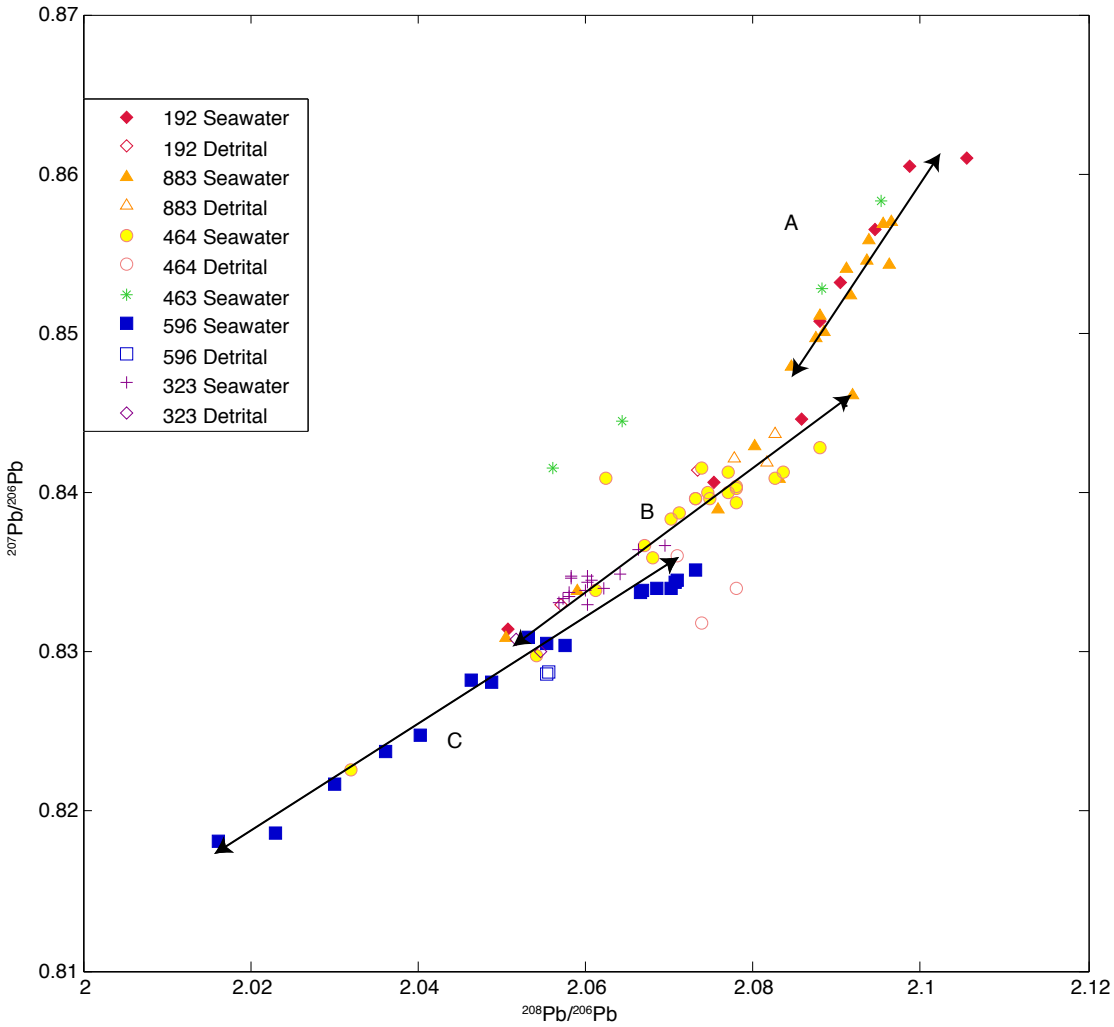

Figure 5.16 $^{207}Pb/^{206}Pb$ versus $^{208}Pb/^{206}Pb$ ratios for study sites, including detrital fractions. Open symbols represent detrital values. The resulting plot reveals two isotopic signatures in the North Pacific sites, marked as arrays A and B, and one in the South Pacific sites, marked by array C, and which carries a similar isotopic signature to array B.

Comparison of seawater and detrital $^{207}Pb/^{206}Pb$ values with $^{208}Pb/^{206}Pb$ values reveals considerable overlap in the isotopic compositions recorded at the study sites. Figure 5.16 indicates three domains of Pb isotopic signatures in the Pacific, marked as arrays A, B, and C (although arrays B and C could be considered a single array given

their similarity). Most of the Northernmost Pacific sites coincide with array A, which comprises the lower end-member values of Site 192, 883, and 463 with $^{206}Pb/^{204}Pb$ values ranging from ~18.12 to 18.38 and $^{208}Pb/^{204}Pb$ values ranging from ~38.03 to 38.37 (Table 5.2). Array B corresponds to the higher end-member compositions of Sites 192, 883 and 464. $^{206}Pb/^{204}Pb$ ratios of Array B range between ~18.48 to 18.89, and $^{208}Pb/^{204}Pb$ values range from ~38.32 to 38.87 (Table 5.2). Array C represents the southern component of Pb in Pacific deep waters, containing the higher end-member values. Array C includes the most radiogenic Pb isotopic values found in this study and is representative of the Southern component of Pacific Pb sources, with $^{206}Pb/^{204}Pb$ ratios ranging from ~18.69 to 19.31 and $^{208}Pb/^{204}Pb$ ratios that range between ~38.47 and 39.13 (Table 5.2).

Although the three arrays each appear well defined, the overlap in values suggests that Pb alone is not particularly diagnostic of provenance. For example, the overlap in values for arrays B and C includes study sites too far apart to be influenced by the same water mass or dust/ash sources. Nevertheless, changes in arrays within individual sites may at least lend some insight into the timing of changes in Pb sources, particularly at Sites 192 and 883.

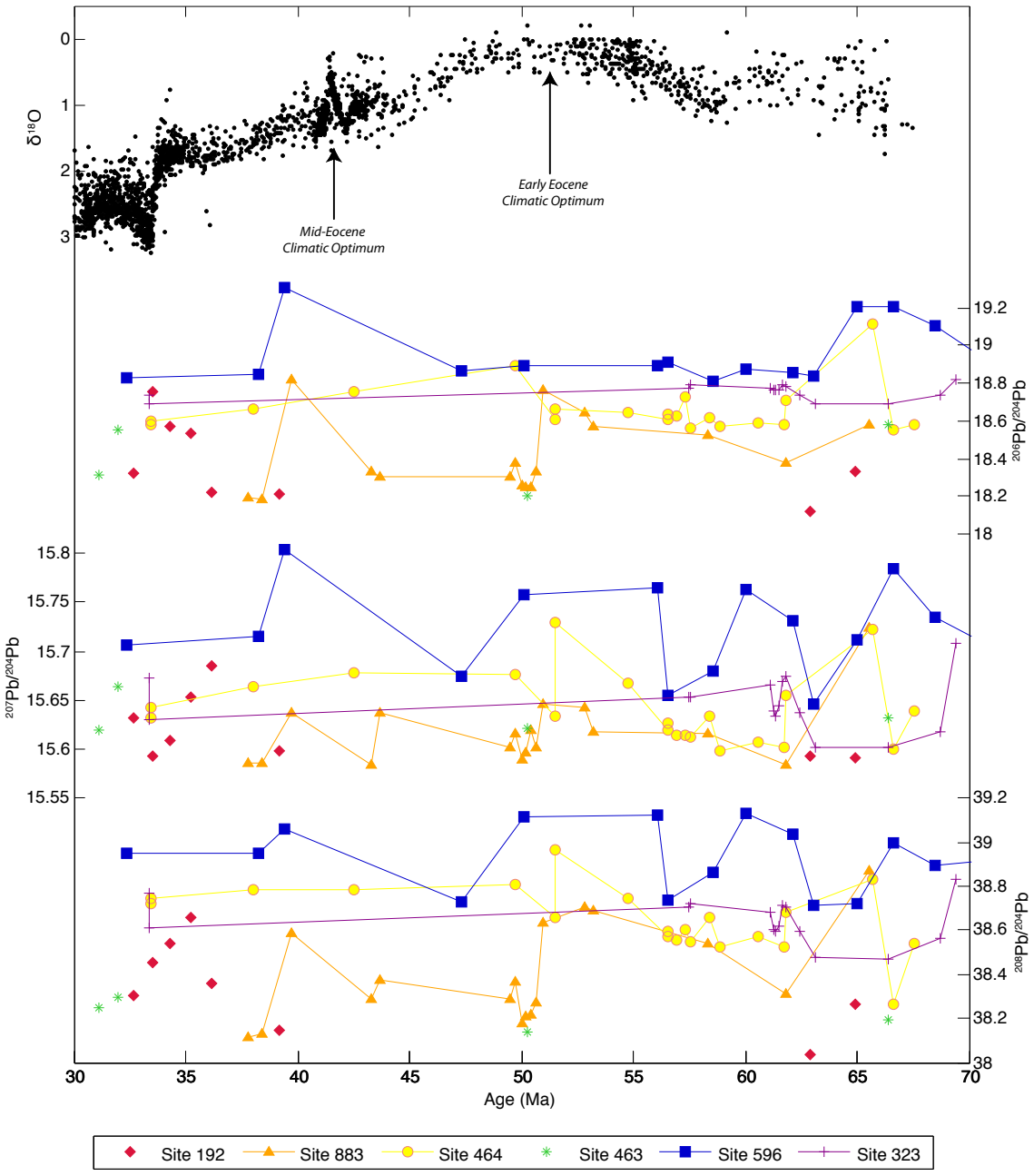

Figure 5.17 Comparison of $^{206,207,208}Pb/^{204}Pb$ ratios of this study to global climate variations. High-resolution deep-sea $\delta^{18}O$ records compiled by Zachos et al. [2008].

To examine the potential relationship between seawater dissolved Pb records and global climate, we compare the three Pb isotope systems to the deep-sea oxygen isotope

records (Fig. 5.17). Northern Pacific Sites 883 and 464 both show clear shifts in $^{206,207,208}Pb/^{204}Pb$ values ~50 Ma, during the peak of Cenozoic warmth known as the early Eocene climatic optimum (EECO) [*Zachos et al.*, 2008]. The shift in values at Site 883 coincides with a switch from array B to array A (Table 5.2). As mentioned before, concordant variations in all three Pb isotopes at Site 883 may be the result of variations in dissolved Pb in the deep-water convection region. Thus, if our previous interpretation of coupled Pb and Nd values in the North Pacific is true, in which dissolved Pb composition was controlled by water mass composition from ~61 to 50 Ma, then the Pb composition of array B in North Pacific sites composed the water mass composition of the convection region for NPDW. $^{207,208}Pb/^{204}Pb$ values at Site 596 also show peak values from ~56 to 50 Ma. Discordancy between $^{207,208}Pb/^{204}Pb$ and $^{206}Pb/^{204}Pb$ values at Site 596, as in 464, is believed to be caused by silicate dust dissolution, thus the peak $^{207,208}Pb/^{204}Pb$ values at Site 596 may be indicative of a dry period in dust source regions during the EECO.

Both Sites 883 and 596 appear to have responded to the middle Eocene climatic optimum (MECO) with increases in values of all three Pb isotope systems. The MECO is characterized by a short negative excursion in $\delta^{18}O$ ~41.5 Ma [*Bijl et al.*, 2010; *Bohaty and Zachos*, 2003]. The increases at Sites 883 and 596 in all three Pb systems may indicate changes in the Pb composition of water masses that advected into their respective locations. The Nd record shows only a slight rise in values during MECO at Site 596, but at Site 883, it shows a significant peak that may coincide with the MECO (Fig 5.6, 5.12). At Site 883, the increase in both Pb and Nd values (and incidentally, a

short-lived divergence to an array-b value in the Pb composition) could have been caused by a short period of re-strengthening in the NPDW while the SPDW may still have been unstable [*Thomas et al.*, 2000]. The increase in values of all three Pb systems at Site 596 suggests the Pb composition was influenced by advected water masses.

Table 5.2 Pb isotopic data generated in this study with corresponding $\varepsilon_{Nd}(t)$ values where applicable. Nd data collected by Hague et al. [2012], and Thomas et al., [in review].

Sample ID	Depth (mbsf)	Age (Ma)	$\varepsilon_{Nd}(t)$	$^{206}Pb/^{204}Pb$	$^{207}Pb/^{204}Pb$	$^{208}Pb/^{204}Pb$	$^{207}Pb/^{206}Pb$	$^{208}Pb/^{206}Pb$	Array
Site 192									
1-1, 52-55	942.52	32.66	-3.5	18.3233	15.6320	38.3045	0.8531	2.0905	a
1-3, 51-53	945.51	33.54	-3.7	18.7533	15.5928	38.4561	0.8315	2.0506	b
1-5, 18-20	948.18	34.33	-3.9	18.5691	15.6089	38.5369	0.8406	2.0753	b
2-1, 66-68	951.66	35.25	-3.4	18.5334	15.6533	38.6589	0.8446	2.0859	b
2-6, 57-59	959.07	36.13	-2.1	18.2172	15.6847	38.3568	0.8610	2.1055	a
3-2, 52-54	985.02	39.22	-2.5	18.2119	15.5988	38.1439	0.8565	2.0944	a
4-2, 92-94	1020.42	62.94	2.2	18.1213	15.5922	38.0335	0.8604	2.0988	a
4-4, 52-54	1023.02	64.94	-1.9	18.3270	15.5913	38.2670	0.8507	2.0880	a
Detrital-192									
1-3, 51-53	945.51	33.54		18.8939	15.7377	38.8641	0.8329	2.0570	b
4-2, 92-94	1020.42	62.94		18.4837	15.5528	38.3258	0.8414	2.0735	b
Site 883									
76-5, 92-94	727.02	37.77		18.1893	15.5866	38.1177	0.8569	2.0956	a
77-1, 28-30	730.18	38.45		18.1860	15.5868	38.1279	0.8571	2.0966	a
77-4, 50-52	734.90	39.73	-2.3	18.8203	15.6382	38.5889	0.8309	2.0504	b
79-2, 20-22	751.20	43.28	-2.2	18.3312	15.5845	38.2856	0.8502	2.0886	a
79-3, 65-67	753.15	43.70	-2.3	18.3037	15.6367	38.3716	0.8543	2.0964	a
82-1, 60-62	779.80	49.49	-1.9	18.3053	15.6027	38.2889	0.8524	2.0917	a
82-2, 50-52	781.20	49.72		18.3793	15.6164	38.3658	0.8497	2.0874	a
82-3, 50-52	783.32	50.06		18.2542	15.5894	38.1735	0.8540	2.0912	a
82-4, 50-52	784.20	50.20		18.2518	15.5969	38.2108	0.8545	2.0935	a
82-5, 50-52	785.70	50.44		18.2513	15.6203	38.2134	0.8558	2.0937	a
82-6, 50-52	787.20	50.67		18.3302	15.6011	38.2748	0.8511	2.0881	a
83-1, 48-50	789.68	50.98		18.7639	15.6461	38.6354	0.8338	2.0590	b
85-1, 60-62	809.50	52.81	-2.1	18.6458	15.6428	38.7061	0.8389	2.0759	b
85-4, 20-22	813.60	53.19	-2.5	18.5720	15.6177	38.6875	0.8409	2.0831	b

Table 5.2 Continued.

Sample ID	Depth (mbsf)	Age (Ma)	$\varepsilon_{Nd}(t)$	$^{206}Pb/^{204}Pb$	$^{207}Pb/^{204}Pb$	$^{208}Pb/^{204}Pb$	$^{207}Pb/^{206}Pb$	$^{208}Pb/^{206}Pb$	Array
86-2, 20-22	820.20	58.36	2.3	18.5261	15.6166	38.5388	0.8430	2.0802	b
86-5, 5-7	824.55	61.80	3.7	18.3776	15.5840	38.3087	0.8480	2.0845	a
87-1, 97-99	829.07	65.56	3.5	18.5831	15.7234	38.8714	0.8461	2.0918	b
Detrital-883									
77-1, 31-33	730.21	38.55		18.5003	15.6083	38.5292	0.8437	2.0826	b
79-3, 65-67	753.15	43.70		18.5623	15.6289	38.6385	0.8420	2.0816	b
86-5, 5-7	824.55	61.80		18.5378	15.6116	38.5187	0.8421	2.0778	b
Site 464									
6-1, 90-92 S	42.40	33.42	-5.2	18.5826	15.6323	38.7207	0.8412	2.0837	b
6-1, 90-92	42.40	33.42	-4.4	18.6018	15.6421	38.7422	0.8409	2.0827	b
6-2, 97-99	43.97	38.05	-3.1	18.6626	15.6647	38.7823	0.8394	2.0781	b
6-3, 100-102	45.50	42.55	-4.4	18.7556	15.6785	38.7859	0.8359	2.0680	b
6-5, 44-46	47.95	49.76	-3.2	18.8920	15.6767	38.8078	0.8298	2.0542	b
6-5, 105-107	48.55	51.53	-3.0	18.6043	15.6334	38.6578	0.8403	2.0779	b
6-5, 105-107	48.55	51.53		18.6616	15.7288	38.9666	0.8428	2.0881	b
6-6, 64-66	49.64	54.74	-1.3	18.6439	15.6675	38.7419	0.8404	2.0780	b
7-1, 50-52	51.50	56.54	-2.0	18.6033	15.6194	38.5687	0.8396	2.0732	b
7-1, 50-52	51.50	56.54	-2.1	18.6324	15.6276	38.5915	0.8387	2.0712	b
7-1, 125-127	52.25	56.91	-1.7	18.6250	15.6140	38.5584	0.8383	2.0703	b
7-2, 60-62	53.10	57.33	-0.3	18.7272	15.6149	38.6013	0.8338	2.0612	b
7-2, 100-102	53.50	57.52	-1.1	18.5580	15.6124	38.5471	0.8413	2.0771	b
7-3, 137-139	55.37	58.44	-0.7	18.6125	15.6336	38.6600	0.8400	2.0771	b
7-4, 70-72	56.20	58.85	-0.6	18.5713	15.5988	38.5265	0.8399	2.0745	b
7-6, 120-122	59.70	60.58	0.2	18.5886	15.6068	38.5677	0.8396	2.0748	b
8-2, 70-72	62.02	61.72	-1.6	18.5827	15.6014	38.5250	0.8396	2.0732	b
8-2, 84-86	62.16	61.79	-1.3	18.7113	15.6544	38.6791	0.8366	2.0672	b
9-1, 4-6	70.04	65.67	-4.6	19.1122	15.7223	38.8340	0.8226	2.0319	c
9-4, 92-94	71.95	66.61	-4.7	18.5519	15.6009	38.2635	0.8409	2.0625	unknown
9-6, 46-48	73.86	67.55	-5.2	18.5833	15.6391	38.5392	0.8416	2.0739	b
Detrital-464									
6-1, 90	42.40	33.42		18.8287	15.6629	39.0469	0.8319	2.0738	unknown
6-3, 100	45.50	42.55		18.7907	15.6710	39.0484	0.8340	2.0781	unknown
8-2, 84	62.16	61.79		18.6703	15.6089	38.6651	0.8360	2.0709	b
Site 463									
6-3, 41-43	41.41	31.14	-4.1	18.3159	15.6197	38.2482	0.8528	2.0883	a
6-4, 148-150	43.98	31.98	-3.9	18.5509	15.6648	38.2978	0.8444	2.0645	unknown
7-2, 123-125	46.23	50.28	-3.9	18.2006	15.6211	38.1356	0.8583	2.0953	a
8-1, 40-42	53.4	66.39	-3.1	18.5753	15.6326	38.1928	0.8416	2.0561	unknown

Table 5.2 Continued.

Sample ID	Depth (mbsf)	Age (Ma)	$\varepsilon_{Nd}(t)$	$^{206}Pb/^{204}Pb$	$^{207}Pb/^{204}Pb$	$^{208}Pb/^{204}Pb$	$^{207}Pb/^{206}Pb$	$^{208}Pb/^{206}Pb$	Array
Site 596									
2-6, 50-52	13.50	32.35	-5.3	18.8316	15.7062	38.9520	0.8340	2.0684	c
2-7, 15-17	14.65	38.25	-5.7	18.8473	15.7157	38.9525	0.8338	2.0667	c
2-CC, 10-12	14.88	39.44	-5.4	19.3053	15.8048	39.0565	0.8187	2.0231	c
3-1, 115-117	16.25	47.35	-5.5	18.8623	15.6737	38.7268	0.8310	2.0531	c
3-2, 14-16	16.74	50.08	-5.1	18.8934	15.7576	39.1147	0.8340	2.0703	c
3-2, 132-134	17.92	56.10	-3.6	18.8945	15.7646	39.1236	0.8343	2.0706	c
3-2, 141-143	18.01	56.55	-5.6	18.9069	15.6558	38.7376	0.8280	2.0489	c
3-3, 31-33	18.41	58.56	-6.1	18.8071	15.6801	38.8644	0.8337	2.0665	c
3-3, 63-65	18.73	60.03	-6.0	18.8766	15.7641	39.1340	0.8351	2.0732	c
3-3, 114-116	19.24	62.17	-5.5	18.8517	15.7317	39.0389	0.8345	2.0708	c
3-3, 137-139	19.47	63.09	-5.9	18.8378	15.6457	38.7169	0.8305	2.0553	c
3-4, 38-40	19.98	65.02	-5.8	19.2059	15.7118	38.7248	0.8181	2.0163	c
3-4, 77-79	20.37	66.61	-5.5	19.2090	15.7847	38.9949	0.8217	2.0300	c
3-4, 123-125	20.83	68.53	-5.4	19.1012	15.7351	38.8949	0.8238	2.0362	c
3-5, 27-29	21.37	70.79	-5.9	18.9121	15.7058	38.9119	0.8305	2.0575	c
3-6, 22-24	22.82	76.91	-5.1	19.0127	15.6824	38.7911	0.8248	2.0403	c
3-6, 123-125	23.83	81.57	-5.5	18.9627	15.7044	38.8055	0.8282	2.0464	c
Detrital-596									
3-2, 132	17.92	56.10		18.8757	15.6416	38.7987	0.8287	2.0555	c
3-3, 63	18.73	60.03		18.8752	15.6429	38.8018	0.8288	2.0557	c
Site 323									
14-2, 60-62	638.10	33.36	-6.3	18.7324	15.6728	38.7659	0.8367	2.0695	c
14-2, 60-62	638.10	33.36		18.6869	15.6301	38.6110	0.8364	2.0662	c
14-2, 107-109	638.57	57.51	-5.6	18.7687	15.6531	38.7041	0.8340	2.0622	c
14-2, 121-123	638.71	57.54	-5.0	18.7927	15.6528	38.7182	0.8329	2.0603	c
15-1, 121-123	656.46	61.09	-5.3	18.7744	15.6649	38.6808	0.8344	2.0603	c
15-2, 64-66	657.39	61.28	-5.1	18.7659	15.6384	38.6068	0.8333	2.0573	c
15-2, 109-111	657.84	61.37	-5.0	18.7666	15.6331	38.5984	0.8330	2.0568	c
15-3, 39-41	658.64	61.53	-5.3	18.7658	15.6448	38.6222	0.8337	2.0581	c
15-3, 115-117	659.40	61.68	-5.3	18.7909	15.6690	38.7094	0.8339	2.0600	c
15-4, 39-41	660.14	61.83	-5.2	18.7816	15.6741	38.7060	0.8345	2.0609	c
16-1, 22-24	664.72	62.43		18.7341	15.6375	38.5955	0.8347	2.0602	c
16-2, 62-64	666.62	63.12	-4.1	18.6935	15.6024	38.4782	0.8346	2.0584	c
17-6, 135-137	682.85	66.37	-4.2	18.6893	15.6010	38.4697	0.8348	2.0584	c
18-2, 15-17	694.65	68.73	-3.7	18.7387	15.6173	38.5649	0.8334	2.0580	c
18-4, 35-37	698.39	69.45		18.8143	15.7080	38.8344	0.8349	2.0641	c

Table 5.2 Continued.

Sample ID	Depth (mbsf)	Age (Ma)	$\varepsilon_{Nd}(t)$	$^{206}Pb/^{204}Pb$	$^{207}Pb/^{204}Pb$	$^{208}Pb/^{204}Pb$	$^{207}Pb/^{206}Pb$	$^{208}Pb/^{206}Pb$	Array
Detrital-323									
14-2 60-62	638.10	33.36		18.8331	15.6330	38.6946	0.8301	2.0546	c
16-1, 22-24	664.72	62.72		18.7712	15.5960	38.5124	0.8309	2.0517	c

6. CONCLUSIONS

The Pb isotopic composition of the Pacific Ocean during the late Cretaceous and early Paleogene indicates changes in weathering patterns occur at all six sites. The range of recorded $^{206,207,208}Pb/^{204}Pb$ values are consistent with previously published Pacific Fe-Mn crust records when taking into account the greater range of latitudes covered by the study sites. The North Pacific sites typically exhibit relatively lower Pb isotope compositions than those in the South Pacific. Variations between the three Pb isotope systems reflect different weathering sources: coincident variations in all three Pb isotopes might track the overall variations in dissolved Pb in the deep-water formation region, while discordant trends between $^{206}Pb/^{204}Pb$ and $^{207,208}Pb/^{204}Pb$ values indicate the dissolution of silicate dust. Higher detrital than seawater values in the northernmost Pacific sites, approaching the seawater composition at Site 464 ~62 Ma suggests a strong contribution of continental dust to the North Pacific reflected in detrital analyses of Sites 192, 883 and 464, and the dissolved Pb composition of Site 464.

Comparisons of the $^{206,207,208}Pb/^{204}Pb$ values of each site to their respective Nd records reveal some interesting features. In the central North Pacific, evidence suggests the Pb composition was likely influenced by the composition of the water mass that advected into the study region from ~62 to 50 Ma, likely due to stronger contribution of NPDW. As convection of NPDW weakened and contributions of deep waters from the South Pacific increased, Pb and Nd decoupled, possibly due to the more distal source of South Pacific deep waters and the stronger influence of dust dissolution above ~50 Ma. Evidence from Site 596 suggests the Pb isotopic composition of the subtropical south

Pacific was influenced by dust dissolution from inputs of westerly winds, while the Nd isotope signature was dominated by the water mass composition. The coupling of Pb and Nd at Site 323 throughout the record indicates the area was probably influenced by the Pb and Nd composition of water masses advected into the region. This is consistent with its proximity to Antarctic source rocks.

A comparison of $^{206,207,208}Pb/^{204}Pb$ records to variations in climate also yields interesting results. Shifts in $^{206,207,208}Pb/^{204}Pb$ values ~50 Ma at Site 883 and 464 occur during the EECO, suggesting the previously discussed shift from regional Pb composition influenced primarily by advected water masses to the Pb composition of eolian inputs was related as well. $^{207,208}Pb/^{204}Pb$ values at Site 596 also show a shift during this time period, and may indicate a dry period in the dust source region. Radiogenic excursions in $^{206,207,208}Pb/^{204}Pb$ values ~40 Ma at Sites 883 and 596 may be related to the mid-Eocene climatic optimum. As the Nd record at Site 883 also reflects this excursion, it is possible that the warming during the MECO caused the NPDW to regain strength and influence the Pb and Nd isotope composition for only a short period of time before reverting to increased deep water contributions from the South Pacific as the Eocene cooling continued. However, a higher-resolution dataset would be needed to determine if such a short warming event would indeed influence the isotopic composition of regional water masses.

REFERENCES

Abouchami, W., and S. Galer (1998), The provinciality of Pb isotopes in Pacific Fe-Mn deposits, *Mineral Magazine*, *62*, 1-2

Abouchami, W., S. L. Goldstein, S. J. G. Gazer, A. Eisenhauer, and A. Mangini (1997), Secular changes of lead and neodymium in central Pacific seawater recorded by a Fe–Mn crust, *Geochimica et Cosmochimica Acta*, *61*(18), 3957-3974

Bains, S., R. M. Corfield, and R. D. Norris (1999), Mechanisms of climate warming at the end of the Paleocene, *Science*, *285*(5428), 724-727

Barker, P. F. (2001), Scotia Sea regional tectonic evolution: implications for mantle flow and palaeocirculation, *Earth-Science Reviews*, *55*(1–2), 1-39

Barker, P. F., and J. Burrell (1977), The opening of Drake passage, *Marine Geology*, *25*(1-3), 15-34

Barrera, E., S. M. Savin, E. Thomas, and C. E. Jones (1997), Evidence for thermohaline-circulation reversals controlled by sea-level change in the latest Cretaceous, *Geology*, *25*(8), 715-718

Barrett, T. J., P. N. Taylor, and J. Lugoqski (1987), Metalliferous sediments from DSDP Leg 92: The East Pacific Rise transect, *Geochimica et Cosmochimica Acta*, *51*(9), 2241-2253

Basak, C., and E. E. Martin (2013), Antarctic weathering and carbonate compensation at the Eocene-Oligocene transition, *Nature Geoscience*, *6*(2), 121-124

Basak, C., E. E. Martin, and G. D. Kamenov (2011), Seawater Pb isotopes extracted from Cenozoic marine sediments, *Chemical Geology*, *286*(3–4), 94-108

Bice, K. L., D. Birgel, P. A. Meyers, K. A. Dahl, K. U. Hinrichs, and R. D. Norris (2006), A multiple proxy and model study of Cretaceous upper ocean temperatures and atmospheric CO2 concentrations, *Paleoceanography*, *21*(2), PA2002

Bijl, P. K., A. J. P. Houben, S. Schouten, S. M. Bohaty, A. Sluijs, G.-J. Reichart, J. S. Sinninghe Damsté, and H. Brinkhuis (2010), Transient Middle Eocene atmospheric CO2 and temperature variations, *Science*, *330*(6005), 819-821

Bijl, P. K., S. Schouten, A. Sluijs, G. J. Reichart, J. C. Zachos, and H. Brinkhuis (2009), Early Palaeogene temperature evolution of the southwest Pacific Ocean, *Nature*, *461*(7265), 776-779

Bohaty, S. M., and J. C. Zachos (2003), Significant Southern Ocean warming event in the late middle Eocene, *Geology*, *31*(11), 1017-1020

Broecker, W. S., R. Gerard, M. Ewing, and B. C. Heezen (1960), Natural radiocarbon in the Atlantic Ocean, *Journal of Geophysical Research*, *65*(9), 2903-2931

Bryden, H. L., H. R. Longworth, and S. A. Cunningham (2005), Slowing of the Atlantic meridional overturning circulation at 25 N, *Nature*, *438*(7068), 655-657

Chen, T.-Y., H.-F. Ling, R. Hu, M. Frank, and S.-Y. Jiang (2013), Lead isotope provinciality of central North Pacific Deep Water over the Cenozoic, *Geochemistry, Geophysics, Geosystems*, *14*(5), 1523-1537

Christensen, J. N., A. N. Halliday, L. V. Godfrey, J. R. Hein, and D. K. Rea (1997), Climate and ocean dynamics and the lead isotopic records in Pacific ferromanganese crusts, *Science*, *277*(5328), 913-918

Coates, A. G., J. B. C. Jackson, L. S. Collins, T. M. Cronin, H. J. Dowsett, L. M. Bybell, P. Jung, and J. A. Obando (1992), Closure of the Isthmus of Panama: the near-shore marine record of Costa Rica and western Panama, *Geological Society of America Bulletin*, *104*(7), 814-828

Cochran, J. K., T. McKibbin-Vaughan, M. M. Dornblaser, D. Hirschberg, H. D. Livingston, and K. O. Buesseler (1990), 210Pb scavenging in the North Atlantic and North Pacific Oceans, *Earth and Planetary Science Letters*, *97*(3–4), 332-352

Coleman, R. G. (1981), Tectonic setting for ophiolite obduction in Oman, *Journal of Geophysical Research*, *86*(B4), 2497-2508

Craig, H., S. Krishnaswami, and B. L. K. Somayajulu (1973), 210Pb 226Ra: Radioactive disequilibrium in the deep sea, *Earth and Planetary Science Letters*, *17*(2), 295-305

Creager, J. S., R. E. Boyce, R. J. Echols, T. J. Fullam, J. A. Grow, I. Koizumi, J. H. Lee, H.-Y. Ling, P. R. Supko, R. J. Stewart, T. R. Worsley, A. Ericson, J. Hess, G. Bryan, R. Stoll, and D. W. Scholl (1971), Initial Reports of the Deep Sea Drilling Project covering Leg 19 of the cruises of the Drilling Vessel Glomar Challenger; Kodiak, Alaska to Yokohama, Japan, July-September 1971, in *Initial Reports of the Deep Sea Drilling Project*, edited by D. W. Scholl, pp. 12-15, American Geological Institute, Alexandria, VA.

Doyle, P. S., and W. R. Riedel (1981), Ichthyoliths at Site 464 in the Northwest Pacific, Deep Sea Drilling Project Leg 62, in *Initial Reports of the Deep Sea Drilling Project*, edited by L. N. e. T. Stout, Joern; Vallier, Tracy L.; Adelseck, Charles G.; Boersma, Anne; Cepek, Pavel; Dean, Walter E.; Fujii, Naoyuki; Koporulin, Vladimir I.; Rea,

David K.; Sancetta, Constance A.; Sayre, William O.; Seifert, Karl E.; Schaaf, Andre; Schmidt, Ronald R.; Windom, Kenneth E.; Vincent, Edith, pp. 491-494, Texas A & M University, Ocean Drilling Program, College Station, TX.

Duce, R. A., P. S. Liss, J. T. Merrill, E. L. Atlas, P. Buat-Menard, B. B. Hicks, J. M. Miller, J. M. Prospero, R. Arimoto, T. M. Church, W. Ellis, J. N. Galloway, L. Hansen, T. D. Jickells, A. H. Knap, K. H. Reinhardt, B. Schneider, A. Soudine, J. J. Tokos, S. Tsunogai, R. Wollast, and M. Zhou (1991), The atmospheric input of trace species to the world ocean, *Global Biogeochemical Cycles*, *5*(3), 193-259

Egenhoff, S. O., and F. Lucassen (2003), Chemical and isotopic composition of Lower to Upper Ordovician sedimentary rocks (Central Andes/South Bolivia): implications for their source, *The Journal of Geology*, *111*(4), 487-497

Erel, Y., Y. Harlavan, and J. D. Blum (1994), Lead isotope systematics of granitoid weathering, *Geochimica et Cosmochimica Acta*, *58*(23), 5299-5306

Finn, C. A., R. D. Müller, and K. S. Panter (2005), A Cenozoic diffuse alkaline magmatic province (DAMP) in the southwest Pacific without rift or plume origin, *Geochemistry, Geophysics, Geosystems*, *6*(2), Q02005

Foster, G. L., and D. Vance (2006), Negligible glacial–interglacial variation in continental chemical weathering rates, *Nature*, *444*(7121), 918-921

Frank, M. (2002), Radiogenic isotopes: Tracers of past ocean circulation and erosional input, *Reviews of Geophysics*, *40*(1), 1-1–1-38

Frank, M. (2011), Geochemical proxies of ocean circulation and weathering inputs: Radiogenic isotopes of Nd, Pb, Sr, Hf, and Os, paper presented at IOP Conference Series: Earth and Environmental Science, IOP Publishing, Montreal, Canada.

Goldstein, S. J., and S. B. Jacobsen (1988), Nd and Sr isotopic systematics of river water suspended material: implications for crustal evolution, *Earth and Planetary Science Letters*, *87*(3), 249-265

Gradstein, F. M., J. G. Ogg, A. G. Smith, W. Bleeker, and L. J. Lourens (2004), A new geologic time scale, with special reference to Precambrian and Neogene, *Episodes*, *27*(2), 83-100

Hague, A. M., D. J. Thomas, M. Huber, R. Korty, S. C. Woodard, and L. B. Jones (2012), Convection of North Pacific deep water during the early Cenozoic, *Geology*, *40*(6), 527-530

Haug, G. H., R. Tiedemann, R. Zahn, and A. C. Ravelo (2001), Role of Panama uplift on oceanic freshwater balance, *Geology*, *29*(3), 207-210

Henderson, G. M., and E. Maier-Reimer (2002), Advection and removal of 210Pb and stable Pb isotopes in the oceans: A general circulation model study, *Geochimica et Cosmochimica Acta*, *66*(2), 257-272

Hole, M. J., P. D. Kempton, and I. L. Millar (1993), Trace-element and isotopic characteristics of small-degree melts of the asthenosphere: Evidence from the alkalic basalts of the Antarctic Peninsula, *Chemical Geology*, *109*(1), 51-68

Hollister, C. D., C. Craddock, Y. A. Bogdanov, N. T. Edgar, J. M. Gieskes, B. U. Haq, J. R. Lawrence, F. Roegl, H.-J. Schrader, B. E. Tucholke, W. R. Vennum, F. M. Weaver, V. N. Zhivago, and P. Worstell (1976), Initial reports of the Deep Sea Drilling Project covering Leg 35 of the cruises of the drilling vessel Glomar Challenger; Callao, Peru to Ushuaia, Argentina, February-March 1974, in *Initial Reports of the Deep Sea Drilling Project*, edited by P. Worstell, p. 929, Texas A & M University, Ocean Drilling Program, College Station, TX.

Huber, B. T., R. D. Norris, and K. G. MacLeod (2002), Deep-sea paleotemperature record of extreme warmth during the Cretaceous, *Geology*, *30*(2), 123-126

Janecek, T. R., and D. K. Rea (1983), Eolian deposition in the northeast Pacific Ocean: Cenozoic history of atmospheric circulation, *Geological Society of America Bulletin*, *94*(6), 730-738

Jones, C. E., A. N. Halliday, D. K. Rea, and R. M. Owen (1994), Neodymium isotopic variations in North Pacific modern silicate sediment and the insignificance of detrital REE contributions to seawater, *Earth and Planetary Science Letters*, *127*(1-4), 55-66

Jones, C. E., A. N. Halliday, D. K. Rea, and R. M. Owen (2000), Eolian inputs of lead to the North Pacific, *Geochimica et Cosmochimica Acta*, *64*(8), 1405-1416

Konstantinovskaia, E. (2001), Arc–continent collision and subduction reversal in the Cenozoic evolution of the Northwest Pacific: an example from Kamchatka (NE Russia), *Tectonophysics*, *333*(1-2), 75-94

Lang Farmer, G., K. Licht, R. J. Swope, and J. Andrews (2006), Isotopic constraints on the provenance of fine-grained sediment in LGM tills from the Ross Embayment, Antarctica, *Earth and Planetary Science Letters*, *249*(1-2), 90-107

Lawver, L. A., and L. M. Gahagan (2003), Evolution of Cenozoic seaways in the circum-Antarctic region, *Palaeogeography, Palaeoclimatology, Palaeoecology*, *198*(1–2), 11-37

Le Pichon, X., R. D. Hyndman, and G. Pautot (1971), Geophysical study of the opening of the Labrador Sea, *Journal of Geophysical Research*, *76*(20), 4724-4743

Ling, H. F., S. Y. Jiang, M. Frank, H. Y. Zhou, F. Zhou, Z. L. Lu, X. M. Chen, Y. H. Jiang, and C. D. Ge (2005), Differing controls over the Cenozoic Pb and Nd isotope evolution of deepwater in the central North Pacific Ocean, *Earth and Planetary Science Letters*, *232*(3), 345-361

Livermore, R., A. Nankivell, G. Eagles, and P. Morris (2005), Paleogene opening of Drake Passage, *Earth and Planetary Science Letters*, *236*(1-2), 459-470

Lugmair, G. W., and S. J. G. Galer (1992), Age and isotopic relationships among the angrites Lewis Cliff 86010 and Angra dos Reis, *Geochimica et Cosmochimica Acta*, *56*(4), 1673-1694

Martin, E. E., S. W. Blair, G. D. Kamenov, H. D. Scher, E. Bourbon, C. Basak, and D. N. Newkirk (2010), Extraction of Nd isotopes from bulk deep sea sediments for paleoceanographic studies on Cenozoic time scales, *Chemical Geology*, *269*(3), 414-431

McArthur, J. M., R. J. Howarth, and T. R. Bailey (2001), Strontium Isotope Stratigraphy: LOWESS Version 3: Best Fit to the Marine Sr−Isotope Curve for 0–509 Ma and Accompanying Look−up Table for Deriving Numerical Age, *The Journal of Geology*, *109*(2), 155-170

McPhaden, M. J., and D. Zhang (2002), Slowdown of the meridional overturning circulation in the upper Pacific Ocean, *Nature*, *415*(6872), 603-608

Menard, H. W., J. H. Natland, T. H. Jordan, J. A. Orcutt, R. G. Adair, M. S. Burnett, I. I. Kim, A. Lerner-Lam, W. Mills, R. Prevot, M. A. Riedesel, M. H. Ritzwoller, E. J. Rosencrantz, P. R. Shaw, P. M. Shearer, D. K. Smith, K. M. Toy, S. Trowell, C. Van Bruggen, R. B. Whitmarsh, D. F. Willoughby, and K. L. Turner (1987), Initial reports of the Deep Sea Drilling Project covering Leg 91 of the cruises of the drilling vessel Glomar Challenger, Wellington, New Zealand, to Papeete, Tahiti, January-February, 1983, in *Initial Reports of the Deep Sea Drilling Project*, edited by K. L. Turner, p. 255, Texas A & M University, Ocean Drilling Program, College Station, TX.

Moll-Stalcup, E. J. (1994), Latest Cretaceous and Cenozoic magmatism in mainland Alaska, in *The Geology of Alaska*, edited by G. Plafker and H. C. Berg, pp. 589-619, Geological Society of America, Boulder, Colorado.

Msadek, R., and C. Frankignoul (2009), Atlantic multidecadal oceanic variability and its influence on the atmosphere in a climate model, *Climate Dynamics*, *33*(1), 45-62

Murphy, M. G., and J. P. Kennett (1986), Development of latitudinal thermal gradients during the Oligocene: oxygen-isotope evidence from the southwest Pacific, in *Initial Reports of the Deep Sea Drilling Project*, edited by J. P. Kennett and C. C. Vonder Borch, et al., pp. 1347-1360.

Nakai, S. i., A. N. Halliday, and D. K. Rea (1993), Provenance of dust in the Pacific Ocean, *Earth and Planetary Science Letters*, *119*(1–2), 143-157

Nriagu, J. O. (1989), A global assessment of natural sources of atmospheric trace metals, *Nature*, *338*(6210), 47-49

O'Nions, R. K., S. R. Carter, R. S. Cohen, N. M. Evensen, and P. J. Hamilton (1978), Pb, Nd and Sr isotopes in oceanic ferromanganese deposits and ocean floor basalts, *Nature*, *273*, 435-438

Olesen, O., J. Ebbing, E. Lundin, E. Mauring, J. R. Skilbrei, T. H. Torsvik, E. K. Hansen, T. Henningsen, P. Midbøe, and M. Sand (2007), An improved tectonic model for the Eocene opening of the Norwegian–Greenland Sea: Use of modern magnetic data, *Marine and Petroleum Geology*, *24*(1), 53-66

Pak, D. K., and K. G. Miller (1992), Paleocene to Eocene benthic foraminiferal isotopes and assemblages: Implications for deepwater circulation, *Paleoceanography*, *7*(4), 405-422

Patterson, C. C., and D. M. Settle (1987), Magnitude of lead flux to the atmosphere from volcanoes, *Geochimica et Cosmochimica Acta*, *51*(3), 675-681

Pearson, P. N., and M. R. Palmer (2000), Atmospheric carbon dioxide concentrations over the past 60 million years, *Nature*, *406*(6797), 695-699

Pettke, T., A. N. Halliday, and D. K. Rea (2002), Cenozoic evolution of Asian climate and sources of Pacific seawater Pb and Nd derived from eolian dust of sediment core LL44-GPC3, *Paleoceanography*, *17*(3), 1031

Pohlmann, H., F. Sienz, and M. Latif (2006), Influence of the multidecadal Atlantic meridional overturning circulation variability on European climate, *Journal of Climate*, *19*(23), 6062-6067

Rea, D. K., I. A. Basov, T. R. Janecek, E. Arnold, J. A. Barron, L. Beaufort, J. F. Bristow, P. deMenocal, G. J. Dubuisson, A. Y. Gladenkov, T. Hamilton, B. L. Ingram, L. D. Keigwin Jr., R. A. Keller, A. T. Kotilainen, L. A. Krissek, B. C. McKelvey, J. J. Morley, M. Okada, G. Olafsson, R. M. Owen, D. K. Pak, T. F. Pedersen, J. A. Roberts, A. K. Rutledge, V. V. Shilov, H. Snoeckx, R. Stax, R. Tiedemann, R. J. Weeks, and A. Palmer-Julson (1993), Proceedings of the Ocean Drilling Program, Initial Reports,

Vol.145, in *Inital Reports of the Ocean Driling Program*, edited, pp. 121-302, Texas A & M University, Ocean Drilling Program, College Station, TX.

Rögl, F., C. D. Hollister, and C. Craddock (1976), Late Cretaceous to Pleistocene foraminifera from the southeast Pacific basin, DSDP Leg 35, in *Initial Reports of the Deep Sea Drilling Project*, edited, pp. 539-555, Washington (US Government Printing Office).

Scher, H. D., and E. E. Martin (2004), Circulation in the Southern Ocean during the Paleogene inferred from neodymium isotopes, *Earth and Planetary Science Letters*, *228*(3–4), 391-405

Searle, M. P., B. F. Windley, M. P. Coward, D. J. W. Cooper, A. J. Rex, D. C. Rex, L. Tingdong, X. Xuchang, M. Q. Jan, and V. C. Thakur (1987), The closing of Tethys and the tectonics of the Himalaya, *Geological Society of America Bulletin*, *98*(6), 678-701

Shackleton, N. J., and J. P. Kennett (1974), Palaeotemperature history of the Cenozoic from oxygen isotope studies in D.S.D.P. Leg 29, in *Marine Plankton and Sediments and Third Planktonic Conference (chaired by Seibold, E.)*, edited, p. 66, Int. Counc. Sci. Unions--UNESCO, Paris.

Shen, G. T., and E. A. Boyle (1988), Determination of lead, cadmium and other trace metals in annually-banded corals, *Chemical Geology*, *67*(1), 47-62

Sigurdsson, H., S. Kelley, R. Leckie, S. Carey, T. Bralower, and J. King (2000), History of circum-Caribbean explosive volcanism: 40Ar/39Ar dating of tephra layers, in *Proceedings of the Ocean Drilling Program, Scientific Results, Vol. 165*, edited, pp. 299-314, Ocean Drilling Program.

Stickley, C. E., H. Brinkhuis, S. A. Schellenberg, A. Sluijs, U. Röhl, M. Fuller, M. Grauert, M. Huber, J. Warnaar, and G. L. Williams (2004), Timing and nature of the deepening of the Tasmanian Gateway, *Paleoceanography*, *19*(4), PA4027

Sun, S. S. (1980), Lead isotopic study of young volcanic rocks from mid-ocean ridges, ocean islands and island arcs, *Philosophical Transactions of the Royal Society of London. Series A, Mathematical and Physical Sciences*, *297*(1431), 409-445

Talwani, M., and O. Eldholm (1977), Evolution of the Norwegian-Greenland sea, *Geological Society of America Bulletin*, *88*(7), 969-999

Tanaka, N., Y. Takeda, and S. Tsunogai (1983), Biological effect on removal of Th-234, Po-210 and Pb-210 from surface water in Funka Bay, Japan, *Geochimica et Cosmochimica Acta*, *47*(10), 1783-1790

Thiede, J., T. L. Vallier, and C. G. Adelseck (1981), Deep Sea Drilling Project Leg 62, North central Pacific Ocean; introduction, cruise narrative, principal results, and explanatory notes, in *Initial Reports of the Deep Sea Drilling Project*, edited by L. N. T. Stout, Joern; Vallier, Tracy L.; Adelseck, Charles G.; Boersma, Anne; Cepek, Pavel; Dean, Walter E.; Fujii, Naoyuki; Koporulin, Vladimir I.; Rea, David K.; Sancetta, Constance A.; Sayre, William O.; Seifert, Karl E.; Schaaf, Andre; Schmidt, Ronald R.; Windom, Kenneth E.; Vincent, Edith, pp. 5-32, Texas A & M University, Ocean Drilling Program, College Station, TX.

Thomas, D. J. (2004), Evidence for deep-water production in the North Pacific Ocean during the early Cenozoic warm interval, *Nature*, *430*(6995), 65-68

Thomas, D. J., T. J. Bralower, and C. E. Jones (2003), Neodymium isotopic reconstruction of late Paleocene–early Eocene thermohaline circulation, *Earth and Planetary Science Letters*, *209*(3), 309-322

Thomas, D. J., M. Lyle, T. C. Moore Jr., and D. K. Rea (2008), Paleogene deepwater mass composition of the tropical Pacific and implications for thermohaline circulation in a greenhouse world, *Geochemistry, Geophysics, Geosystems*, *9*(2), Q02002

Thomas, D. J., J. A. Schubert, B. Haines, R. Korty, and M. Huber (in review), Pacific Deep-water Circulation Separate From Atlantic During the Latest Cretaceous - Early Cenozoic, edited.

Thomas, E., J. C. Zachos, and T. J. Bralower (2000), Deep-sea environments on a warm Earth: Latest Paleocene–early Eocene, *Warm Climates in Earth History*, 132-160

Todt, W., R. Cliff, A. Hanser, and A. Hofmann (1996), Evaluation of a 202Pb-205Pb double spike for high-precision lead isotope analysis, paper presented at Washington DC American Geophysical Union Geophysical Monograph Series.

Torsvik, T. H., and L. R. M. Cocks (2005), Norway in space and time: a centennial cavalcade, *Norwegian Journal of Geology*, *85*(1-2), 73-86

Trocine, R. P., and J. H. Trefry (1988), Distribution and chemistry of suspended particles from an active hydrothermal vent site on the Mid-Atlantic Ridge at 26 N, *Earth and Planetary Science Letters*, *88*(1-2), 1-15

van de Flierdt, T., M. Frank, A. N. Halliday, J. R. Hein, B. Hattendorf, D. Günther, and P. W. Kubik (2003), Lead isotopes in North Pacific deep water–implications for past changes in input sources and circulation patterns, *Earth and Planetary Science Letters*, *209*(1-2), 149-164

van de Flierdt, T., F. Martin, N. H. Alex, R. H. James, H. Bodo, G. Detlef, and W. K. Peter (2004), Deep and bottom water export from the Southern Ocean to the Pacific over the past 38 million years, *Paleoceanography*, *19*(1), PA1020

Via, R. K., and D. J. Thomas (2006), Evolution of Atlantic thermohaline circulation: Early Oligocene onset of deep-water production in the North Atlantic, *Geology*, *34*(6), 441-444

von Blanckenburg, F., and T. F. Nägler (2001), Weathering versus circulation-controlled changes in radiogenic isotope tracer composition of the Labrador Sea and North Atlantic Deep Water, *Paleoceanography*, *16*(4), 424-434

von Blanckenburg, F., R. K. O'nions, and J. R. Heinz (1996), Distribution and sources of pre-anthropogenic lead isotopes in deep ocean water from Fe□ Mn crusts, *Geochimica et Cosmochimica Acta*, *60*(24), 4957-4963

Wilson, T. J. (1992), Mesozoic and Cenozoic kinematic evolution of the Transantarctic Mountains, in *Recent Progress in Antarctic Earth Science*, edited by Y. T. K. Kaminuma, pp. 303-314, Terra Science, Tokyo.

Zachos, J., G. R. Dickens, and R. E. Zeebe (2008), An early Cenozoic perspective on greenhouse warming and carbon-cycle dynamics, *Nature*, *451*(7176), 279-283

Zachos, J., M. Pagani, L. Sloan, E. Thomas, and K. Billups (2001), Trends, rhythms, and aberrations in global climate 65 Ma to present, *Science*, *292*(5517), 686-693

Zachos, J., T. M. Quinn, and K. A. Salamy (1996), High-resolution (104 years) deep-sea foraminiferal stable isotope records of the Eocene-Oligocene climate transition, *Paleoceanography*, *11*(3), 251-266

Zhou, L., and F. T. Kyte (1992), Sedimentation history of the South Pacific pelagic clay province over the last 85 million years inferred from the geochemistry of Deep Sea Drilling Project Hole 596, *Paleoceanography*, *7*(4), 441-465

Ziegler, P. A. (1987), Late Cretaceous and Cenozoic intra-plate compressional deformations in the Alpine foreland—a geodynamic model, *Tectonophysics*, *137*(1-4), 389-420